

SELF-CONSISTENT MODELS OF THE AGN AND BLACK HOLE POPULATIONS: DUTY CYCLES, ACCRETION RATES, AND THE MEAN RADIATIVE EFFICIENCY

FRANCESCO SHANKAR¹, DAVID H. WEINBERG¹ AND JORDI MIRALDA-ESCUDE²

Draft version February 11, 2013

ABSTRACT

We construct evolutionary models of the populations of active galactic nuclei (AGN) and supermassive black holes, in which the black hole mass function grows at the rate implied by the observed luminosity function, given assumptions about the radiative efficiency and the luminosity in Eddington units. We draw on a variety of recent X-ray and optical measurements to estimate the bolometric AGN luminosity function and compare to X-ray background data and the independent estimate of Hopkins et al. (2007) to assess remaining systematic uncertainties. The integrated AGN emissivity closely tracks the cosmic star formation history, suggesting that star formation and black hole growth are closely linked at all redshifts. We discuss observational uncertainties in the local black hole mass function, which remain substantial, with estimates of the integrated black hole mass density ρ_{\bullet} spanning the range $3 - 5.5 \times 10^5 M_{\odot} \text{Mpc}^{-3}$. We find good agreement with estimates of the local mass function for a reference model where all active black holes have a fixed efficiency $\epsilon = 0.065$ and $L_{\text{bol}}/L_{\text{Edd}} \approx 0.4$ (shifting to $\epsilon = 0.09$, $L_{\text{bol}}/L_{\text{Edd}} \approx 0.9$ for the Hopkins et al. luminosity function). In our reference model, the duty cycle of $10^9 M_{\odot}$ black holes declines from 0.07 at $z = 3$ to 0.004 at $z = 1$ and 10^{-4} at $z = 0$. The decline is shallower for less massive black holes, a signature of “downsizing” evolution in which more massive black holes build their mass earlier. The predicted duty cycles and AGN clustering bias in this model are in reasonable accord with observational estimates. If the typical Eddington ratio declines at $z < 2$, then the “downsizing” of black hole growth is less pronounced. Models with reduced Eddington ratios at low redshift or black hole mass predict fewer low mass black holes ($M_{\bullet} \lesssim 10^8 M_{\odot}$) in the local universe, while models with black hole mergers predict more black holes at $M_{\bullet} > 10^9 M_{\odot}$. Matching the integrated AGN emissivity to the local black hole mass density implies $\epsilon = 0.075 \times (\rho_{\bullet}/4.5 \times 10^5 M_{\odot} \text{Mpc}^{-3})^{-1}$ for our standard luminosity function estimate, or 25% higher for Hopkins et al.’s estimate. It is difficult to reconcile current observations with a model in which most black holes have the high efficiencies $\epsilon \approx 0.16 - 0.20$ predicted by MHD simulations of disk accretion. We provide electronic tabulations of our bolometric luminosity function and our reference model predictions for black hole mass functions and duty cycles as a function of redshift.

Subject headings: cosmology: theory – black hole: formation – galaxies: evolution – quasars: general

1. INTRODUCTION

The long-standing hypothesis that quasars are powered by accretion onto supermassive black holes (Salpeter 1964; Lynden-Bell 1969; Rees 1984) is now strongly supported by many lines of evidence, including the apparent ubiquity of remnant black holes in the spheroids of local galaxies (Richstone et al. 1998). The strong correlations between the masses of central black holes and the luminosities, dynamical masses, and velocity dispersions of their host spheroids (e.g., Magorrian et al. 1998; Ferrarese & Merritt 2000; McLure & Dunlop 2002; Marconi & Hunt 2003; Häring & Rix 2004; Ferrarese & Ford 2005; Greene & Ho 2006; Graham 2007; Hopkins et al. 2007b; Shankar & Ferrarese 2008; Shankar et al. 2008) imply that the processes of black hole growth and bulge formation are intimately linked. Theoretical models typically tie black hole growth to episodes of rapid star formation, perhaps associated with galaxy mergers, and ascribe the black hole-bulge correlations to energy or momentum feedback from the black hole or to regulation of black hole growth by the bulge potential (e.g., Silk & Rees 1998; Kauffmann & Haehnelt 2000; Cavaliere & Vittorini 2000; Granato et al. 2004, 2006; Murray, Quataert, & Thompson 2004; Cattaneo et al. 2005; Miralda-Escudé & Kollmeier 2005; Monaco & Fontanot 2005; Croton et al. 2006; Hopkins et al. 2006a, Mal-

bon et al. 2006). These correlations also make it possible to estimate the mass function of black holes in the local universe (e.g., Salucci et al. 1999; Yu & Tremaine 2002; Marconi et al. 2004; Shankar et al. 2004, S04 hereafter). This local mass function provides important constraints on the co-evolution of the quasar and black hole populations. The most general and most well known of these constraints is the link between the integrated emissivity of the quasar population, the integrated mass density of remnant black holes, and the average radiative efficiency of black hole accretion (Soltan 1982; Fabian & Iwasawa 1999; Elvis et al. 2002).

In the paper we construct self-consistent models of the quasar population using a method that can be considered a “differential” generalization of Soltan’s (1982) argument. Given assumed values of the radiative efficiency and the Eddington ratio L/L_{Edd} , the observed luminosity function of quasars at a given redshift can be linked to the average growth rate of black holes of the corresponding mass, and these growth rates can be integrated forward in time to track the evolution of the black hole mass function. This modeling approach has been developed and applied in a variety of forms by numerous authors, drawing on steadily improving observational data (e.g. Cavaliere et al. 1973; Small & Blandford 1992; Salucci et al. 1999; Cavaliere & Vittorini 2000; Yu & Tremaine 2002; Steed & Weinberg 2003, hereafter SW03; Hosokawa 2004; Yu & Lu 2004; Marconi et al. 2004; S04; Merloni 2004; Vittorini, Shankar & Cavaliere 2005; Tamura

¹ Astronomy Department, Ohio State University, Columbus, OH-43210, U.S.A.

² Institut de Ciències de L’Espai (IEEC-CSIC)/ICREA, Bellaterra, Spain

et al. 2006; Hopkins et al. 2007). The consensus of recent studies is that evolutionary models with radiative efficiencies of roughly 10% and mildly sub-Eddington accretion rates yield a reasonable match to the observational estimates of the remnant mass function. However, uncertainties in the bolometric luminosity function of active galactic nuclei (AGN, a term we will use to describe both quasars and less luminous systems powered by black hole accretion) and in the local black hole mass function remain an important source of uncertainty in these conclusions.

We begin our investigation by constructing an estimate of the bolometric AGN luminosity function. Our estimate starts from the model of Ueda et al. (2003, hereafter U03), based on data from several X-ray surveys, but we adjust its parameters based on more recent optical and X-ray data that provide more complete coverage of luminosity and redshift. Comparison to the X-ray background and to the independent luminosity function estimate of Hopkins, Richards & Hernquist (2007; HRH07 hereafter) gives an indication of the remaining uncertainties, associated mainly with bolometric corrections and the fraction of obscured sources. In agreement with Marconi et al. (2004) and Merloni (2004), we find similar trends in the evolution of AGN emissivity and the cosmic star formation rate, supporting models in which the growth of black holes occurs together with the formation of stars in their hosts (e.g., Sanders et al. 1988; Granato et al. 2004; Hopkins et al. 2006a). We also reassess current estimates of the local black hole mass function, finding that different choices and calibrations of the black hole-bulge correlation lead to significantly different results, with integrated mass densities that span nearly a factor of two.

Our simplest models of the evolving black hole and AGN populations assume that all active black holes have a single radiative efficiency ϵ and a single accretion rate \dot{m} in Eddington units. The work of Kollmeier et al. (2006) suggests that a constant value of \dot{m} may be a reasonable approximation for luminous quasars, but the observational evidence on this point is mixed (e.g., McLure & Dunlop 2004; Vestergaard 2004; Babic et al. 2007; Bundy et al. 2007; Netzer & Trakhtenbrot 2007; Netzer et al. 2007; Rovilos & Gorgantopoulos 2007; Shen et al. 2007b), and for lower luminosity, local AGN there is clearly a broad range of Eddington ratios (e.g., Heckmann et al. 2004). We also consider models in which \dot{m} depends on redshift or black hole mass, and we consider a simple model of black hole mergers to assess their potential impact on the mass function. We will examine models with distributions of \dot{m} values and a more realistic treatment of mergers in future work.

Our modeling allows a consistency test of the basic scenario in which the observed luminosity of black hole accretion drives the growth of the underlying black hole population, and comparison to the local black hole mass function yields constraints on the average radiative efficiency and the typical accretion rate. For specified ϵ and \dot{m} , the model predicts the black hole mass function as a function of time, and combination with the observed luminosity function yields the duty cycle as a function of redshift and black hole mass. These predictions can be tested against observations of AGN host galaxy properties and AGN clustering, and they can be used as inputs for further modeling. While significant uncertainties remain, we find that a simple model of the black hole and AGN populations achieves a good match to a wide range of observational data.

2. THE AGN BOLOMETRIC LUMINOSITY FUNCTION

In order to constrain the accretion history of black holes, it is essential to know the shape and evolution with redshift of the AGN bolometric LF. The determination of this LF is not straightforward, as it must be made using the AGN LF *observed* in particular bands and converted into bolometric estimates using empirically calibrated bolometric corrections. The bolometric corrections have been shown by several authors to be redshift independent, with some possible trend with the intrinsic luminosity of the source (e.g., Elvis et al. 1994; Marconi et al. 2004; Richards et al. 2006; Hopkins et al. 2007a). AGN surveys have been carried out at several energy ranges, and in each one the detection of sources can be highly affected by intrinsic or instrumental selection effects. In different ranges of redshift and luminosity, the best statistics come from different wavebands or surveys, further complicating the effort to create a comprehensive AGN LF.

An additional challenge in assembling a reliable and complete census of the AGN population is obscuration of the central engine by gas and dust, which may reside in the “molecular torus” of unified models (Antonucci 1993) or in the interstellar medium of the galactic host (Martinez-Sansigre et al. 2005; Rigby et al. 2006). Strong obscuration can eliminate sources from surveys entirely, while uncorrected weak obscuration causes their luminosities to be underestimated. For solar composition gas, the absorption optical depth to X-ray photons is $\tau = 2.04(N_H/10^{22} \text{ cm}^{-2})(E/1 \text{ keV})^{-2.4}$ (e.g., Kembhavi & Narlikar 1999). For Galactic dust-to-gas ratio, the extinction in the rest-frame visual band is $A_V = 5.35 \text{ mag} \times (N_H/10^{22} \text{ cm}^{-2})$ (e.g., Binney & Merrifield 2000). Hard X-ray selection is thus the least affected by obscuration, and deep X-ray surveys indeed reveal many faint AGNs that are missed by traditional optical selection criteria (e.g., Hasinger et al. 2005). Numerous studies suggest that the incidence of obscuration decreases towards high intrinsic luminosity, so that X-ray and optical LFs agree at the bright end but diverge at low luminosities (e.g., U03; Richards et al. 2005; La Franca et al. 2005; Hasinger et al. 2005). Statistically speaking, there is fairly good correspondence between X-ray AGNs with $\log N_H/\text{cm}^{-2} \leq 22$ and broad-line optical AGNs (e.g., Tozzi et al. 2006). Even 2-10 keV selection becomes highly incomplete for Compton-thick sources, with $\log N_H/\text{cm}^{-2} \geq 24$, and the best constraints on this population come from the normalization and spectral shape of the X-ray background.

Given these considerations, we have chosen to base our bolometric LF estimate principally on the work of U03, who compiled a vast sample from *Chandra*, *ASCA*, and *HEAO-1* surveys and inferred the absorption-corrected LF in the rest-frame 2-10 keV band out to $z \sim 3$. We adopt the luminosity-dependent bolometric correction of Marconi et al. (2004); we include a dispersion of 0.2 dex in this correction (see, e.g., Elvis et al. 1994), but omitting the scatter would not significantly affect our results. U03 fit their data with a parameterized model of luminosity-dependent density evolution. We adopt the model and adjust its parameters in some redshift ranges to better fit other data sets, especially at high redshifts and at bright luminosities at low redshifts. We note that many other studies have reported general trends of the LF evolution and obscuring columns similar to those of U03 (e.g., La Franca et al. 2005), and that infrared surveys also suggest a substantial population of obscured AGNs at low luminosities (Treister et al. 2006; see also Ballantyne and Papovich 2007).

The number of sources per unit volume per dex of luminosity $\log L_X = \log L_{2-10\text{keV}}$ is fitted by U03 using a double power-law multiplied by an “evolution” term:

$$\Phi(L_X, z) = e(z, L_X) \frac{A}{\left(\frac{L_X}{L^*}\right)^{\gamma_1} + \left(\frac{L_X}{L^*}\right)^{\gamma_2}}, \quad (1)$$

where

$$e(L_X, z) = \begin{cases} (1+z)^{p_1} & \text{if } z < z_c(L_X) \\ (1+z_c)^{p_1} [(1+z)/(1+z_c(L_X))]^{p_2} & \text{if } z \geq z_c(L_X) \end{cases}, \quad (2)$$

with

$$z_c(L_X) = \begin{cases} z_c^* & \text{if } L_X \geq L_a \\ z_c^* (L_X/L_a)^{0.335} & \text{if } L_X < L_a \end{cases}. \quad (3)$$

We tune the value of parameters in order to provide a good fit to the overall set of data presented in Figure 1. The full list of parameters is given in Table 1. Some of the parameters assume different values in different redshift intervals, in which case we apply a linear interpolation in z between these intervals, as reported in Table 1. The X-ray LF of equation (1) is converted into a bolometric LF using the fit to the bolometric correction given by Marconi et al. (2004), $\log L/L_X = 1.54 + 0.24\zeta + 0.012\zeta^2 - 0.0015\zeta^3$ with $\zeta = \log L/L_\odot - 12$, and $L_\odot = 4 \times 10^{33} \text{ erg s}^{-1}$, then convolved with a Gaussian scatter of dispersion 0.2 dex to account for dispersion in the bolometric correction. We find the bright-end slope γ_2 should vary with time to match the data, steepening at very low redshifts ($z \leq 0.8$) and at high ($z \geq 4$) redshifts. We caution that the “evolution” term $e(L_X, z)$ substantially modifies the shape of the luminosity function below $L \approx 10^{45} \text{ erg s}^{-1}$. For example, the effective LF slope in the range $10^{43} \text{ erg s}^{-1} \leq L \leq 10^{44.5} \text{ erg s}^{-1}$ changes from -1.4 at $z \sim 2$ to -0.7 at $z \sim 0$ even though we keep γ_1 (appearing in equation [1]) fixed at 0.86.

Figure 1 compares our model of the AGN LF to a large collection of data from optical surveys (Pei 1995; Wisotzki 1999; Fan et al. 2001, 2004; Kennefick et al. 1994; Hunt et al. 2004; Wolf et al. 2003; Richards et al. 2005, 2006; Jiang et al. 2006; Cool et al. 2006; Bongiorno et al. 2007; Fontanot et al. 2007; Shankar & Mathur 2007) and X-ray surveys (Barger et al. 2003; Ueda et al. 2003; Barger & Cowie 2005; Barger et al. 2005; La Franca et al. 2005; Nandra et al. 2005; Silverman et al. 2008). Optical data have been converted from the B -band into bolometric quantities using $L_{\nu_B} \nu_B C_B = L$, where L_{ν_B} is the monochromatic luminosity at $\nu_B = 6.8 \times 10^{14} \text{ Hz}$ ($\sim 4400 \text{ \AA}$). We use an average value of $C_B = 10.4$ consistent with Richards et al. (2006). Note that Marconi et al. (2004) and Hopkins et al. (2007; HRH07 hereafter) suggest values 30%-50% lower depending on luminosity, while Elvis et al. (1994) proposed a higher value of 11.8. In Figure 1 we plot $L\Phi(L)$, instead of simply $\Phi(L)$ itself, to highlight the luminosity bins where most of the energy is emitted. For the same reason, we will later plot the black hole mass function as $M_\bullet \Phi(M_\bullet)$ to highlight the mass bins in which most of the density resides.

The dot-dashed curves in Figure 1 show our model LF including only sources with $\log N_H/\text{cm}^{-2} \leq 22$, which we calculate using the luminosity-dependent column density distribution functions of U03. The dashed curves show the contribution of all sources with $\log N_H/\text{cm}^{-2} \leq 24$, while the solid curves include higher column density (Compton-thick) systems. We assume that the number of Compton-thick sources in each luminosity bin is equal to the number of sources in

the column density range $23 \leq \log N_H/\text{cm}^{-2} \leq 24$. We will henceforth follow the X-ray convention of describing systems with $\log N_H/\text{cm}^{-2} < 22$ as “Type I” AGN and systems with $22 \leq \log N_H/\text{cm}^{-2} \leq 24$ as Type II AGN. We roughly expect the “Type I” curve (dot-dashed) to agree with optical survey data points and the “Type I+Type II” curve to agree with X-ray survey data points. The agreement between the model and the data is overall fairly good, though in some regimes different data sets give seemingly incompatible results, making it difficult to judge the validity of the model itself.

HRH07 have used their observationally constrained theoretical models to estimate the fraction of AGN that are “missing” from observational samples because of obscuration, as a function of waveband and luminosity. In Figure 2, we plot data points corrected for these obscured fractions, with the same model curves as Figure 1. If the data, the obscuration corrections, and our model were all perfect, then all of the data points should line up with each other and with the solid model curves. The obscuration corrections do reduce the discrepancies among data sets, most notably in the range $z \approx 0.7 - 3.2$, but they do not remove all of the differences. The upper envelope of the data points is generally close to our model near the peak of $L\Phi(L)$, though at the highest luminosities the model exceeds the data (principally SDSS) for $z \approx 0.7 - 2.0$.

In Figure 3 we show the integrated intensity obtained from our model AGN LF compared with all the available data on the cosmic X-ray Background (XRBG) for energies above 1 keV. The data are a collection of old and new results presented by Frontera et al. (2007), plus the recent results from *INTEGRAL* (Churazov et al. 2006). While the shape of the XRBG is now well established at low energies (2-10 keV band), different studies imply normalizations that differ by up to 40%. The minimum estimate for the normalization was found by the very first *HEAO* experiments (e.g., Marshall et al. 1980; filled circles in Figure 3), while the much more recent *Chandra* and *XMM* results point towards higher values (shaded bands in Figure 3; see Comastri 2004 for a review). Several groups have assumed that the *HEAO* measurements were correct in shape but underestimated in normalization because of flux calibration and/or instrumental background subtraction (Frontera et al. 2007), implying a true XRBG spectrum that is ~ 1.4 times the *HEAO* spectrum at all energies. However, recent measurements from *INTEGRAL* (Churazov et al. 2006; open circles in Figure 3) and from the *PDS* instrument aboard *BeppoSAX* (Frontera et al. 2007) produce results close to the original *HEAO* measurements in the ~ 20 -100 keV range. Based on the agreement of multiple experiments in overlapping energy ranges, we tentatively conclude that the true XRBG spectrum approximately follows the *INTEGRAL* points over the range ~ 5 -100 keV.

The solid curve in Figure 3 shows the XRBG predicted by our AGN bolometric LF model with the U03 column density distribution. Following U03, we use the PEXRAV code (Magdziarz & Zdziarski 1995) to generate spectra of families of AGN with different column densities, also taking into account Compton down-scattering for highly obscured sources (Wilman & Fabian 1999). We compute the spectra of Compton-thick ($\log N_H/\text{cm}^{-2} > 24$) sources assuming $\log N_H/\text{cm}^{-2} = 24.5$. Dashed, dot-dashed, and triple-dot-dashed curves show the cumulative contributions of sources with $\log N_H/\text{cm}^{-2} < 22, 23$, and 24, respectively. The Compton-thick sources increase the predicted XRBG by a factor of about 1.3 at $E \gtrsim 20 \text{ keV}$, with smaller contribu-

tions at lower energies and at much higher energies. Our full model would be a good match to the *HEAO* spectrum renormalized by a constant factor of ~ 1.4 as proposed in some earlier studies. However, it significantly overpredicts the *INTEGRAL* and *SAX/PDS* results at $E > 10$ keV; these are well matched by the contribution of $\log N_H/\text{cm}^{-2} \leq 24$ sources alone, with *no* Compton-thick contribution. As noted above, we employ U03's prescription for the luminosity dependence of the Compton-thick fraction. If we use a simpler model in which the number of Compton-thick sources is 40% of the number of $\log N_H/\text{cm}^{-2} \leq 24$ sources at all luminosities, then we obtain very similar XRBG predictions (higher by a few percent near the peak and even closer at other energies).

We conclude from Figure 3 that the Compton-thick fraction in our standard model is probably an upper limit on the true fraction, and in our calculations below we will also consider a model in which the Compton-thick fraction is zero. However, Gilli et al. (2007) have proposed a successful model to fit the *INTEGRAL* measurements of the XRBG that uses a combined contribution from unobscured sources (which they define to be only those with $\log N_H/\text{cm}^{-2} \leq 21$) a factor ~ 2 below our estimate and a higher contribution from obscured sources up to $\log N_H/\text{cm}^{-2} = 26$, which they derive by assuming that these sources have a Gaussian distribution of spectral indices around a mean slope $\langle \Gamma \rangle = 1.9$. With this result in mind, we will also explore models with a higher fraction of Compton-thick sources (but our standard estimate of unobscured sources).

Reproducing the high background normalization found by *XMM* in the 2-5 keV range would require a substantially higher contribution from Type I AGN, since obscured AGN have little emission at these energies. Such an increase seems implausible on other grounds. Following Schirber & Bullock (2003) and Miralda-Escudé (2003), we have estimated the average hydrogen ionization rate produced by Type I X-ray AGN with optical luminosity $M_B \leq -15$ assuming UV spectral energy index $\alpha_{UV} = 1.57$. Using the redshift-dependent X-ray-to-optical ratio by Steffen et al. (2006), we find that the Type I AGNs produce an emissivity that saturates the estimated UV background intensity at $z \lesssim 1$. We therefore conclude that the true AGN contribution to the XRBG is probably closer to our model prediction than to the *XMM* band shown in Figure 3. If future missions confirm a high normalization of the XRBG in the 2-5 keV range, it would probably mean that a substantial contribution from X-ray binaries in normal galaxies is present at these energies. On the other hand, we note from Figure 1 that our AGN LF defined for sources with $\log N_H/\text{cm}^{-2} \leq 22$ is consistent with, or even lower than, all optical survey estimates, so we do not expect a much *lower* contribution from these sources.

HRH07 have recently undertaken an exercise similar to ours, attempting to construct a bolometric AGN LF that is consistent with a wide range of data over a large span of energies and wavelengths. Figure 4 compares our model to theirs. We find good agreement in the shape and overall normalization of the AGN LF in the redshift range $z < 1$ and $3.5 \leq z \leq 4.5$, while at intermediate redshifts our model LF is systematically lower. The normalization difference arises because HRH07 adopt an X-ray bolometric correction that is about 30% higher (at typical luminosities) than the Marconi et al. (2004) bolometric correction used here. If we adopt the HRH07 bolometric correction, then we find good agreement in the range $1 \leq z \leq 3$, but our model LF is higher at high and low redshifts. At $z \geq 4$ we adopt a steeper bright-

end LF slope based on the results of GOODs (Fontanot et al. 2006), Cool et al. (2006) and Shankar & Mathur (2007), who find evidence for a steeper slope relative to the estimates of Richards et al. (2006). However, at $1 \leq z \leq 2.5$ the HRH07 bright-end slope is steeper than ours, since they effectively require a match to the SDSS-based measurements of Richards et al. (2004) in this redshift range, while we retain the shallower slope adopted by U03, also supported by recent X-ray LF determination of Silverman et al. (2008). Recent Spitzer studies (Hickox et al. 2007; Polletta et al. 2008) suggest a significant fraction of obscured AGN even at high luminosities, leaving some room for a slope difference between the optical and bolometric LFs. We regard the differences between our model LF and that of HRH07, derived from independent attempts to match the full range of current data, as a reasonable representation of the remaining systematic uncertainties in determination of the bolometric AGN luminosity function. We will show in § 4.3 that the difference between these two determinations does not alter our overall conclusions, but the differences in normalization and shape at intermediate redshifts do lead to different preferred accretion parameters for the black hole population.

3. THE LOCAL BLACK HOLE MASS FUNCTION AND THE INTEGRATED SOLTAN ARGUMENT

3.1. The local black hole mass function

Marconi et al. (2004) and S04 found similar results for the local black hole mass function, using somewhat different methods. Both groups found that starting from the relation between black hole mass and bulge velocity dispersion ($M_\bullet - \sigma$) or the relation between black hole mass and bulge luminosity ($M_\bullet - L_{\text{sph}}$) led to similar local mass functions. However, a more recent analysis by Lauer et al. (2007a) and Tundo et al. (2007) argues that these two methods do not provide the same answer. We therefore revisit some of the uncertainties in computing the local mass function.

Figure 5 compares the local mass functions obtained using different relations between black hole mass and host galaxy properties. Following S04, we start with the galaxy LF in the r^* band by Nakamura et al. (2002), who used light concentration parameters to distinguish early and late type galaxies and derived LFs for both. After correcting the Petrosian magnitudes to total magnitudes by adding -0.2 mag, we convert the LF into a LF of spheroids, which we compute as follows. First we compute the numerical fraction of Elliptical-S0 (spirals Sab-Sbc-Scd) in the early-type (late-type) galaxy LF, then correct each morphological galaxy type for its respective spheroidal luminosity component, as given in Table 1 of Fukugita et al. (1998) for the r -band (see also Yu & Tremaine 2002 and Marconi et al. 2004). Note that this method is equivalent to correcting the luminosities themselves adopting an average weighted fraction of $f_{\text{sph}} = 0.83 - 0.85$ for early-type galaxies, and $f_{\text{sph}} = 0.27 - 0.3$ for late-type galaxies, as done in S04 (and references therein).

The solid line in Figure 5 shows our result using the $M_\bullet - L_{\text{sph}}$ relation calibrated by McLure & Dunlop (2002; their equation 6) for a sample of 18 black holes in inactive galaxies, where we correct the magnitudes for our cosmology. Using the calibration in equation (A9) of Tundo et al. (2006) would give a similar result. These calculations yield a black hole mass function $\sim 34\%$ higher than that in S04 (shown with solid squares). We include a Gaussian scatter of 0.3 dex around the mean $M_\bullet - L_{\text{sph}}$ relation in both cases. The intrinsic scatter to insert in the local relations between black

hole mass and host galaxy properties is empirically uncertain because it is similar in magnitude to the observational uncertainties themselves. However, most authors estimate a scatter of about 0.3 dex, which is close to the value predicted in the numerical simulations of Hopkins et al. (2007b). In the following we will always adopt this value of the scatter for all our computations of the local mass function.

If we instead use the galaxy velocity dispersion function and the $M_\bullet - \sigma$ relation in equation (A5) of Tundo et al. (2006), with a scatter of 0.3 dex, we get the short-dashed line in Figure 5, close to the central estimate of S04. Here we use the velocity dispersion function by Sheth et al. (2003), which includes their estimate for the contribution of the bulges in spirals, which in turn accounts for $\sim 25\%$ of the total estimated black hole mass density. The Sheth et al. (2003) estimate of the velocity dispersion function is in very good agreement with the velocity function estimated by S04 through the bivariate relation of galaxy luminosity and velocity dispersion. However, using the $M_\bullet - \sigma$ relation in Marconi et al. (2004) yields the dot-dashed line, which is higher than the S04 determination by about $1 - \sigma$. The $M_\bullet - \sigma$ relation given in Ferrarese & Ford (2005) is steeper than the Tundo et al. (2007) relation, and adopting it yields a similar mass density to S04, but a local mass function shifted towards higher masses, shown with a triple-dot dashed line in Figure 5 (see also Wyithe 2004). Both of these estimates yield a local mass function below the $M_\bullet - L_{\text{sph}}$ -based local mass function estimate at $M_\bullet < 10^{7.5} M_\odot$, as also noted by S04.

In the following we will adopt the grey band of Figure 5, which spans the range of these estimates, as representative of the mean and the systematic uncertainties of present estimates of the local mass function. The integrated mass density of the local black hole population is $\rho_\bullet = (3.2 - 5.4) \times 10^5 M_\odot \text{Mpc}^{-3}$ (for $h = 0.7$). Figure 5 also presents three additional estimates of the local mass function. Stars show the results of combining the Bell et al. (2003) galaxy baryonic mass function (corrected for spheroid fraction as above) with the Häring & Rix (2004) estimate of the relation between black hole mass and spheroid stellar mass, again assuming 0.3 dex intrinsic scatter. This result is in reasonable agreement with the $M_\bullet - \sigma$ estimates, though uncertainties in the stellar mass-to-light ratio are a remaining source of systematic uncertainty. The dotted curve shows the estimate of Hopkins et al. (2007b), based on a “fundamental plane” relation between black hole mass, galaxy velocity dispersion, and spheroid half-light radius; it is more sharply peaked than the grey band and implies a higher integrated black hole mass density. Open circles show Graham et al.’s (2007) estimate based on the correlation between black hole mass and the Sérsic light-profile index of the galaxy spheroid. This estimate is similar to Hopkins et al.’s (2007b) near the peak, but it implies an even sharper fall off towards low black hole masses. Further discussion of the discrepancies in local mass function estimates, and possible routes to alleviate them, will appear in Shankar & Ferrarese (in preparation).

3.2. The integrated mass density

Before turning to the evolution of the differential black hole mass function, the central theme of this paper, we briefly revisit the classic Sothman (1982) argument, which relates the integrated black hole density to the integrated emissivity of the AGN population. If the average efficiency of converting accreted mass into bolometric luminosity is $\epsilon \equiv L/\dot{M}_{\text{inflow}} c^2$,

where \dot{M}_{inflow} is the mass accretion rate, then the actual accretion onto the central black hole is $\dot{M}_\bullet = (1 - \epsilon)\dot{M}_{\text{inflow}}$, where the factor $1 - \epsilon$ accounts for the fraction of the incoming mass that is radiated away instead of being added to the black hole. The rate at which mass is added to the black hole mass function is then given by

$$\frac{d\rho_\bullet}{dt} = \frac{1 - \epsilon}{\epsilon c^2} \int_0^\infty \Phi(L) L d \log L. \quad (4)$$

The mass growth rate implied by equation (4) and our estimate of the AGN LF from §2 is shown by the solid line in Figure 6a. We set the radiative efficiency to a value of $\epsilon = 0.075$, as it provides a cumulative mass density in agreement with the median estimate of the local mass density discussed in § 3.1. At each time step we integrate equation (4) down to the observed faint-end cut in the 2 – 10 keV AGN LF, which we parameterize as

$$\log L_{\text{MIN}, 2-10\text{keV}}(z) = \log L_{0, 2-10\text{keV}} + 2.5 \log(1 + z). \quad (5)$$

We set $\log L_{2-10\text{keV}}/(\text{erg s}^{-1}) = 41.5$, in agreement with the faintest low redshift objects observed by U03 and La Franca et al. (2005). For a typical L_{opt}/L_X , equation (5) yields an optical luminosity of $M_B \sim -22$ at $z \sim 6$, comparable to the faintest AGN sources observed by Barger et al. (2003) in the 2 Msec Chandra Deep Field North (see also Figure 1 and Shankar & Mathur 2007). At each time step we compute the minimum observed luminosity given in equation (5) and convert it into a bolometric quantity $L_{\text{MIN}}(z)$ applying the adopted bolometric correction by Marconi et al. (2004).

Dashed and dot-dashed lines in Figure 6a show two recent estimates of the cosmic star formation rate (SFR) as a function of redshift, from Hopkins & Beacom (2006), reported with its $3-\sigma$ uncertainty region (dark area), and Fardal et al. (2007). We have multiplied both estimates by a redshift-independent factor of 8×10^{-4} . Since local estimates imply a typical ratio $M_\bullet/M_{\text{star}} \sim 1.6 \times 10^{-3}$ for spheroids (e.g., Häring & Rix 2004), this is a reasonable scaling factor if roughly 50% of star formation goes into spheroidal components (see also Marconi et al. 2004 and Merloni et al. 2004). The agreement between the inferred histories of black hole growth and star formation suggests that the two processes are intimately linked. In particular this association seems to hold down to the last several Gyrs, even at $z \lesssim 1.5$ when disk galaxies are expected to dominate the SFR. A possible link between black hole growth and star formation in disks could arise from re-activations induced by tidal interactions between satellite and central galaxies (e.g., Vittorini et al. 2005). Also, bars could possibly funnel gas into the central black hole, though empirical studies cast some doubt on this mechanism as a primary trigger for black hole growth (Peeples & Martini 2006 and references therein).

Figure 6b presents the same comparison in integrated form (see also De Zotti et al. 2006 and Hopkins et al. 2006b). Solid squares show the black hole mass density obtained by converting the $z = 1$ and $z = 2$ galaxy stellar mass function into a black hole mass function by assuming a ratio $M_\bullet/M_{\text{star}}$ equal to the local one (i.e., 1.6×10^{-3}). The galaxy stellar mass function has been computed from the Caputi et al. (2006) K-band galaxy luminosity function, assuming an average mass-to-light ratio $M_{\text{star}}/L_K = 0.4$ at $z = 1$ and $M_{\text{star}}/L_K = 0.3$ at $z = 2$. The latter values have been obtained from the *Pegase2* code (Fioc & Rocca-Volmerange 1997) by taking a short burst of star formation ($< 10^9$ yr) and a Kennicutt double power-law stellar Initial Mass Function. The quoted values for M_{star}/L_K

can be taken as lower limits, as other choices of the parameters in the code would tend to increase their value. However, we also note that our result on the stellar mass function is in good agreement with the recent estimate by Fontana et al. (2006). Our scaling factor of 1.6×10^{-3} implicitly assumes that all the stellar mass in the luminous galaxies probed by these high-redshift observations resides in spheroidal components today, and is therefore associated with black hole mass.

Figure 6 suggests that the ratio of black hole growth to SFR is approximately the same at all redshifts, and suggests a close link between black hole accretion and star formation. If the average ratio of black hole mass to stellar mass were much higher than the local value at $z = 1 - 2$, then the squares in Figure 6b would shift above the black hole mass density curve $\rho_\bullet(z)$. Increasing M_{star}/L_K would move the squares higher still, while associating only a fraction of the high-redshift stellar mass with present day spheroids would move them lower. Our conclusions are in marginal agreement with those of McLure et al. (2006) and Shields et al. (2006) and in some disagreement with those of Peng et al. (2006), who find $M_\bullet/M_{\text{star}}$ in gravitationally lensed quasar hosts at $z \sim 1 - 2$ a factor ~ 3 above the local value. However, several observational biases may effect studies of the $M_\bullet/M_{\text{star}}$ ratio in high redshift quasar samples (Lauer et al. 2007b). Uncertainties in the local normalization of ρ_\bullet and in the stellar mass-to-light ratios still leave a fair amount of wiggle room, but our results in Figure 6 disfavor models in which black holes “grow first” and spheroid star formation “catches up” at later times. Alternatively, if the average efficiency ϵ of black hole accretion is lower at high redshifts, then the $\rho_\bullet(z)$ curve in Figure 6b would shift upwards at these redshifts accordingly.

4. EVOLVING THE BLACK HOLE MASS FUNCTION

4.1. Method

Our goal is to calculate the evolution of the black hole mass function implied by the bolometric AGN LF described in §2, given assumptions about the radiative efficiency and the typical accretion rate. In the following we will use the symbol $\Phi(x)$ to denote mass and luminosity functions in logarithmic units of L or M_\bullet , i.e.

$$\Phi(x) = n(x)x \ln(10), \quad (6)$$

where $n(x)$ is the comoving space density of black holes in the mass or luminosity range $x \rightarrow x + dx$, in units of Mpc^{-3} for $h = 0.7$.

We define the Eddington accretion rate to be

$$\dot{M}_{\text{Edd}} \equiv \frac{L_{\text{Edd}}}{0.1 c^2} \simeq 22 \left(\frac{M_\bullet}{10^9 M_\odot} \right) M_\odot \text{yr}^{-1} \quad (7)$$

and the dimensionless accretion rate $\dot{m} = \dot{M}_\bullet / \dot{M}_{\text{Edd}}$, where L_{Edd} is the standard Eddington luminosity (for Thomson scattering opacity and pure hydrogen composition) at mass M_\bullet . The black hole growth rate \dot{M}_\bullet is related to the large scale accretion rate by $\dot{M}_\bullet = (1 - \epsilon) \dot{M}_{\text{inflow}}$, where $L = \epsilon \dot{M}_{\text{inflow}} c^2$, because a fraction ϵ of the mass is radiated away before entering the black hole. We define $f = \epsilon / (1 - \epsilon)$, and $f_{0.1} = f / 0.1$, so that a black hole of mass M_\bullet growing at a dimensionless rate \dot{m} has bolometric luminosity

$$L = \epsilon \dot{M}_{\text{inflow}} c^2 = 0.1 f_{0.1} \dot{M}_\bullet c^2 = f_{0.1} \dot{m} l M_\bullet, \quad (8)$$

where $l \equiv L_{\text{Edd}} / M_\bullet = 1.26 \times 10^{38} \text{erg s}^{-1} M_\odot^{-1}$. Note that we define \dot{M}_{Edd} for $f = 0.1$, so the mass Eddington ratio \dot{m} is

linked to the luminosity Eddington ratio λ by the radiative efficiency, i.e.

$$\lambda \equiv \frac{L}{L_{\text{Edd}}} = \dot{m} f_{0.1}. \quad (9)$$

A black hole accreting at a constant value of \dot{m} grows exponentially in time with a timescale $t_{\text{growth}} = M_\bullet / \dot{M}_\bullet = t_s / \dot{m} = 4.5 \times 10^7 \dot{m}^{-1} \text{yr}$, where t_s is equal to the Salpeter (1964) timescale for $f_{0.1} = 1$.

The evolution of the black hole mass function $n(M_\bullet, t)$ is governed by a continuity equation (Cavaliere et al. 1973, Small & Blandford 1992)

$$\frac{\partial n}{\partial t}(M_\bullet, t) = - \frac{\partial(M_\bullet \langle \dot{m} \rangle n(M_\bullet, t))}{\partial M_\bullet}, \quad (10)$$

where $\langle \dot{m} \rangle$ is the mean dimensionless accretion rate (averaged over the active and inactive populations) of the black holes of mass M_\bullet at time t . This evolution is equivalent to the case in which every black hole grows constantly at the mean accretion rate $\langle \dot{m} \rangle$. In practice, individual black holes turn on and off, and there may be a dispersion in \dot{m} values, but the mass function evolution depends only on the mean accretion rate as a function of mass.

All models in this paper assume a single accretion rate $\dot{m} = \dot{m}_0$. At any given time, a black hole is either accreting at \dot{m}_0 or not accreting. In some models we allow the characteristic accretion rate \dot{m}_0 to depend on z , or on M_\bullet . The assumption of a single \dot{m} is clearly not valid for low luminosity AGNs in the nearby universe, which have a wide range of Eddington ratios (e.g., Heckman et al. 2004, Greene & Ho 2007). However, Kollmeier et al. (2005) find that luminous AGN at $0.5 < z < 3.5$ have a narrow range of Eddington ratios, with a peak at $\lambda \sim 1/4$ and a dispersion of 0.3 dex. Since this dispersion includes contributions from random errors in black hole mass estimates and bolometric corrections, the true dispersion should be even smaller. Netzer et al. (2007) find a similar result, with a slightly larger dispersion, from a sample centered at $z \sim 2.5$. We will consider models with multiple \dot{m} values in future work, but single- \dot{m} models (also adopted by, e.g., Marconi et al. 2004 and S04) are a good starting point for understanding black hole growth.

If there is a single accretion rate \dot{m}_0 , then the duty cycle of black hole activity (i.e., the probability that a black hole of mass M_\bullet is active at a particular time) is given by the ratio of luminosity and mass functions,

$$P_0(M_\bullet, z) = \frac{\Phi(L, z) \left| \frac{d \log L}{d \log M_\bullet} \right|}{\Phi(M_\bullet, z)} \leq 1, \quad (11)$$

where $M_\bullet = L / (f_{0.1} \dot{m}_0 l)$ is the black hole mass that corresponds to luminosity L . Models with constant \dot{m}_0 and ϵ have $L \propto M_\bullet$, making the Jacobian factor unity. A physically consistent model must have $P_0(M_\bullet, z) \leq 1$; there must be enough black holes to produce the observed luminous AGNs.

Our strategy is to start with an assumed black hole mass function $n(M_\bullet, z_i)$ at an initial redshift z_i , then track the characteristic curves $M_\bullet(M_{\bullet, i}, z)$ of equation (10) by direct integration

$$M_\bullet(M_{\bullet, i}, z) = \int_{z_i}^z \langle \dot{m}_\bullet \rangle M_\bullet(z') \frac{dt}{dz'} dz' \\ = \int_{z_i}^z \dot{m}_0 P_0(M_\bullet, z') M_\bullet(z') \frac{dt}{dz'} dz'. \quad (12)$$

Here $P_0(M_\bullet, z')$ is given by equation (11) with the observed luminosity function, and the evolved $n(M_\bullet, z)$ is given by

$$n(M_\bullet, z) = n(M_{\bullet,i}, z_i) \frac{dM_{\bullet,i}}{dM_\bullet}, \quad (13)$$

where M_\bullet is the black hole mass that corresponds to initial mass $M_{\bullet,i}$. To put this calculation in more physical terms: we take advantage of the fact that equation (10) is equivalent to having every black hole grow at the rate $\langle \dot{m}(M_\bullet, z) \rangle$. Starting with a set of logarithmically spaced initial values of $M_{\bullet,i}$, we integrate the masses forward in time with a mid-point scheme from redshift step z_j to step $z_{j+1} = z_j - \Delta z$

$$M_{\bullet,j+1} = M_{\bullet,j} + \dot{m}_0 P_0(M_{\bullet,j+1/2}, z_{j+1/2}) M_{\bullet,j+1/2} \frac{dt}{dz} \Delta z, \quad (14)$$

where the values at the mid-point $j + 1/2$ are evaluated by extrapolating black hole masses for a half step $\Delta z/2$ using dM_\bullet/dt at the beginning of the step and the duty cycle P_0 is computed using the mid-step mass function and the luminosity function evaluated at $z_{j+1/2} = z_j + \Delta z/2$. We choose sufficiently small redshift steps Δz such that the total mass density added at each iteration matches the one obtained by integration of the bolometric luminosity function (equation 4), and we have confirmed that smaller Δz yields essentially identical results. Since the number of black holes is conserved, $n(M_\bullet, z) \Delta M_\bullet = n(M_{\bullet,i}, z) \Delta M_{\bullet,i}$.

As an aside, we note that this approach is mathematically equivalent to solving the continuity equation in the form

$$\frac{\partial n(M_\bullet, t)}{\partial t} = - \frac{\dot{m}_0}{t_s \ln(10)^2 M_\bullet} \frac{\partial \Phi(L, z)}{\partial \log L} \quad (15)$$

used by, e.g. Small & Blandford (1992) and Marconi et al. (2004). Equation (15) follows from equation (10) with the assumption of a single \dot{m}_0 and $f_{0.1}$, and it is also valid in the case of a redshift dependent \dot{m}_0 . From equation (15), it is explicitly clear that the evolution of the black hole mass function depends only on the initial conditions, the observed luminosity function, and the values of \dot{m}_0 and $f_{0.1} = L/(M_\bullet \dot{m}_0)$, given the assumptions made here. The Sołtan argument (§ 3.2) relates the integrated black hole mass density to the integrated emissivity of the AGN population. The continuity equation yields the full evolution of the black hole mass function in terms of the full luminosity function; in essence, it applies the Sołtan argument as a function of mass. We have checked that our method yields consistent results against direct integration of the equation.

For our integrations, we generally start at $z_i = 6$ and determine $n(M_{\bullet,i}, z_i)$ from equation (14) with our estimate of the luminosity function at $z = 6$ and an assumed $P_0 = 0.5$. This relatively high initial duty cycle implies we start with nearly the minimal black hole mass function required to reproduce the luminosity function. By $z \sim 3.5$ the integration has essentially forgotten the initial value of P_0 unless we set it much lower (e.g., $P_0 < 0.01$), since the accreted mass is much larger than the mass in the initial black hole population. The clustering of luminous AGN at $z \sim 3 - 4$ implies duty cycles of at least several percent (Shen et al. 2007; Shankar et al., in preparation). In our standard calculations, we set P_0 to zero for masses $M_{\bullet, \text{MIN}}(z)$ that would produce AGN luminosities below the minimum observed luminosity at that redshift (indicated by the cutoffs in Figure 1); we do not extrapolate the luminosity function below these minimum values. Since $L_{\text{MIN}}(z)$ drops towards lower z , we must have a supply

of black holes in place to provide AGNs of lower luminosity as these become visible. To ensure this, we set our initial black hole mass function to

$$n(M_{\bullet,i}, z_i) = 8 \times n(M_{\bullet, \text{MIN}}(z_i), z_i) \times \left(\frac{M_\bullet}{M_{\bullet, \text{MIN}}(z_i)} \right)^{-2.3}, \quad (16)$$

i.e., below $M_{\bullet, \text{MIN}}(z_i)$ we boost $n(M_\bullet, z_i)$ by a factor of 8 and add an $M_\bullet^{-2.3}$ rise (see Figure 7, below). This high initial abundance of low mass black holes ensures that we are never forced to duty cycles $P_0 > 1$. Once M_\bullet significantly exceeds $M_{\bullet, \text{MIN}}(z)$, the black hole mass function is dominated by growth rather than initial values, and $n(M_\bullet, z)$ is insensitive to the assumed $n(M_{\bullet,i}, z_i)$. We adopted this procedure so that our results would not depend on the extrapolation of the luminosity function into regions where it is not observed. In practice, we find that extrapolating the luminosity function as a power law down to very faint luminosities yields similar results. We follow the L_{min} procedure for our standard models in §§ 4.2 and 4.3, and use extrapolation of the LF in §§ 4.4-4.6 where it gives more stable numerical solutions.

4.2. The reference model

Figure 7 shows the results of our calculations for a reference model with our standard estimate of the AGN bolometric luminosity function and accretion parameters $\dot{m} = 0.60$ and $\epsilon = 0.065$ ($f_{0.1} \sim 0.7$), which yield good overall agreement with the average estimate of the local black hole mass function. Panel 7a shows the evolution of the mass function starting from the initial condition at $z = 6$ (solid triangles) and continuing through to $z = 0$. Because of the luminosity-dependent density evolution in the observed luminosity function, the massive end of the black hole mass function builds up early, and the lower mass regime grows at later redshifts. For $M_\bullet > 10^{8.5} M_\odot$, the mass function is almost fully in place by $z = 1$. Panel 7b plots $M_\bullet \Phi(M_\bullet)$, proportional to the fraction of black hole mass per logarithmic interval of M_\bullet , which allows better visual comparison to the observed local mass function and highlights the contribution of each black hole mass bin to the total mass density at each time. The accretion model agrees well with our estimate of the local mass function (grey band) up to $\sim 10^{9.3} M_\odot$. At higher masses our model exceeds the observational estimate, but in this regime the estimate relies on extrapolation of the scaling relations, and it is sensitive to the assumed intrinsic scatter. In addition, the high-mass end of the predicted mass function is sensitive to the bright end of the LF at $z \lesssim 2$ (see § 4.3). The open circles with error bars show the estimate of the local mass function by Graham et al. (2007), which we cannot reproduce even approximately with constant \dot{m}_0 . If this estimate is correct, then the low end of the luminosity function must be produced mainly by high mass black holes accreting at low \dot{m} , so that the predicted growth of low mass black holes is reduced (see § 4.5).

Figure 7c plots the duty cycle as a function of mass for different redshifts, as labeled. The duty cycle for $M_\bullet \sim 10^9 M_\odot$ is ~ 0.2 at $z \sim 4 - 5$, falling to 0.03-0.08 at $z = 2 - 3$, when quasar activity is at its peak, then dropping to 0.003 at $z = 1$ and $\sim 10^{-4}$ at $z = 0$. Below $z \sim 3$, the duty cycle rises towards low black hole masses. This “downsizing” evolution, in which high mass black holes complete their growth early but low mass black holes continue to grow at late times, is required by the observed LF evolution in any model with approximately constant \dot{m}_0 . Above $10^9 M_\odot$ the duty cycle curves are generally flat, because the constant slope of the

bright end of the LF drives the growth of a mass function with a parallel slope. Below $z = 1$, the LF slope changes, and the duty cycle curves are no longer flat. By running several cases with varying initial conditions, we find that the duty cycles for $z \lesssim 3.5$ are insensitive to the assumed initial duty cycle (which determines the initial mass function) provided $0.01 \lesssim P_0(z=6) \leq 1$.

Several lines of independent observational evidence have set constraints on the duty cycle of AGNs at different redshifts. Porciani et al. (2004), Croom et al. (2005), Porciani and Norberg (2006), and da Angela et al. (2006) have analyzed large samples of optical AGNs in the Two Degree Field (2dF) QSO Redshift Survey, showing that their large-scale ($\gtrsim 1$ Mpc) clustering properties are consistent with quasars residing in very massive halos with $M_h \sim 5 \times 10^{12} - 10^{13} M_\odot$. Comparing the AGN abundance to the abundance of such halos implies duty cycles of order of $\sim (1 - 4)\%$ in the redshift range $z \sim 1 - 2$. Similar results have been confirmed by large-scale optical AGN clustering studies in the Sloan Digital Sky Survey (SDSS; e.g., Myers et al. 2007). Shen et al. (2007) have extended the SDSS results to $z = 3 - 4$, obtaining similar results for halo masses and duty cycles. Similar or lower values for the duty cycle could be found directly by comparing the AGN number density to the galaxy luminosity function at comparable redshifts, the latter now well estimated and complete down to rather low luminosities (e.g., Pannella et al. 2006). Using *Chandra* X-ray observations of the Hubble Field North, Nandra et al. (2002) and Steidel et al. (2002) find that about 3% of a large spectroscopic survey of ~ 1000 Lyman Break Galaxies at the average redshift of $z \sim 3$ host an X-ray bright, moderately obscured AGN. Within the uncertainties of the comparison, these estimates of AGN duty cycles are in good agreement with the predictions in Figure 7c. We will present predictions for AGN clustering bias in § 5 below, and we will carry out quantitative comparisons to observed clustering in future work. The occurrence of AGN in massive star-forming galaxies is much higher than these overall duty cycle estimates (Alexander et al. 2003; Borys et al. 2005), supporting the scenario in which star-formation in massive galaxies is closely related to black hole growth (e.g., Granato et al. 2006).

Figure 7d shows the black hole accretion histories as a function of relic mass and redshift, following equation (12). Tracing back one of these curves shows the mass that a “typical” black hole of present mass M_\bullet had at earlier times, as predicted by our model. The dot-dashed line shows the minimum black hole mass associated with $L_{\text{MIN}}(z)$ at each redshift. By construction, all growth curves are flat (dashed lines) before crossing $L_{\text{MIN}}(z)$. Figure 7d shows again that high mass black holes build their mass early and experience little growth at late times, while lower mass black holes grow rapidly at lower redshifts.

4.3. Parameter variations

The top panels of Figure 8 show the effect of varying the two main model parameters, the radiative efficiency ϵ and accretion rate \dot{m}_0 . Figure 8a compares models with varying ϵ and accretion rate fixed to the reference model value $\dot{m} = 0.60$. Lowering (raising) the radiative efficiency has the effect of shifting the accreted mass function up (down) and shifting the peak of the mass distribution to higher (lower) masses. Recall that the luminosity Eddington ratio is $\lambda = \dot{m} f_{0.1}$; if we held λ fixed instead of \dot{m} , then curves in Figure 8a would be vertically displaced with no horizontal shift. Figure 8b shows

models with varying \dot{m}_0 , all with $\epsilon = 0.065$. The Soltan argument implies that $\rho_\bullet = \int M_\bullet \Phi(M_\bullet) d \log M_\bullet$ should be the same for models with the same ϵ that reproduce the same observed LF. The area under the curves in Figure 8b is thus the same for all models, but the peak in the mass function shifts to lower M_\bullet for higher \dot{m}_0 because a given observed luminosity is associated with a lower black hole mass. While there are still systematic uncertainties in the normalization and shape of the local mass function, the peak of the $M_\bullet \Phi(M_\bullet)$ distribution (Figure 5) is in good agreement among all the estimates, and this, in turn, sets strong constraints on \dot{m}_0 . Shifting the peak of the accreted mass distribution to $\log(M_\bullet/M_\odot) \sim 8$ would require Super-Eddington accretion rates, while shifting it to $\log(M_\bullet/M_\odot) \sim 9$ requires $\dot{m}_0 \sim 0.2 - 0.3$. Changes to ϵ and \dot{m}_0 shift the accreted mass function in different directions in the $M_\bullet \Phi(M_\bullet) - M_\bullet$ plane, but they do not alter its shape.

The lower panels of Figure 8 show the effect of changing the input LF. In panel 8c, solid and dotted curves show models with no Compton-thick sources or a double fraction of Compton-thick sources, respectively, with radiative efficiency and accretion rate fixed at the reference model values $\epsilon = 0.065$ and $\dot{m}_0 = 0.6$. The predicted black hole mass functions are similar in shape but offset in amplitude by about $\pm 20\%$. These offsets are similar to our estimated uncertainty in the local mass function, shown by the grey band. We can restore agreement between the double Compton-thick model and the central estimate of the local mass function by raising ϵ to 0.08 (to produce more luminosity with the same black hole mass) and lowering \dot{m}_0 to 0.5 (to compensate the influence of higher ϵ on the peak location). Conversely, the no-Compton-thick model yields similar predictions if ϵ is lowered to 0.05 and \dot{m}_0 is raised to 0.8. As noted in § 2, we find better agreement with the observed X-ray background for no Compton-thick and worse agreement for double Compton-thick (see Figure 3).

Figure 8d compares our reference model to the one obtained by integrating the AGN bolometric LF of HRH07. For the reference model values $\epsilon = 0.065$ and $\dot{m}_0 = 0.6$, the predicted mass function shifts to higher normalization and higher peak mass (solid line). Principally this difference reflects the higher bolometric correction adopted by HRH07, which shifts their LF to higher normalization at $1 \lesssim z \lesssim 3$ (Figure 4). The HRH07 estimate also has higher peak luminosity in this redshift range, leading to higher peak mass. Adopting a higher efficiency and accretion rate, $\epsilon = 0.09$ and $\dot{m}_0 = 1$, largely compensates these two effects. As noted in § 2, the HRH07 LF has a steeper bright-end slope at intermediate redshifts, and this leads to a steeper high-mass slope of the accreted mass function, improving agreement with observational estimates above $M_\bullet \sim 10^9 M_\odot$.

To present our model comparison in a more global way, we characterize the local mass function by four quantities that contain complementary information:

- The integrated black hole mass density $\rho_\bullet = \int M_\bullet \Phi(M_\bullet) d \log M_\bullet$.
- The location $\log M_{\text{PEAK}}$ at which the mass function peaks in the $M_\bullet \Phi(M_\bullet) - M_\bullet$ plane.
- The width of the mass function, characterized by $(\Delta \log M_\bullet)_{1/2}$ such that twice the integral from $\log M_{\text{PEAK}}$ to $\log M_{\text{PEAK}} + (\Delta \log M_\bullet)_{1/2}$ contains half the total mass density, $2 \times$

$\int_{\log M_{\text{PEAK}}}^{\log \bar{M}_\bullet} \Phi(M_\bullet) M_\bullet d \log M_\bullet = 1/2 \times \rho_\bullet$. If $M_\bullet \Phi(M_\bullet)$ were a Gaussian, $(\Delta \log M_\bullet)_{1/2}$ would be ~ 0.26 times the full width at half maximum.

- The asymmetry of the mass function, characterized by $\Delta \rho_\bullet / \rho_\bullet$, the normalized difference in the mass density integrated above and below $\log M_{\text{PEAK}}$.

Figure 9 plots the predicted values of these four quantities as a function of the radiative efficiency ϵ for models with our standard AGN LF and accretion rates $\dot{m}_0 = 1, 0.6, 0.45, 0.3$. Grey horizontal bands show the observational estimates corresponding to the grey band in Figure 5. Short-dashed and long-dashed horizontal lines show instead the parameters for the local mass functions inferred by Graham et al. (2007) and Hopkins et al. (2007b), respectively (see Figure 5). As expected from the Soltan argument, the predicted ρ_\bullet is proportional to $(1 - \epsilon)/\epsilon$ but independent of \dot{m}_0 . Consistency with the grey band observational estimate requires $0.063 \leq \epsilon \leq 0.1$.³ Reproducing the observed value of $\log M_{\text{PEAK}}/M_\odot \approx 8.5$ then requires $0.4 \lesssim \dot{m}_0 \lesssim 0.8$, though for any given ϵ the value of \dot{m}_0 is determined to $\sim 10\%$. As noted in our discussion of Figure 8a, the location of the mass function peak is determined by $\lambda = L/L_{\text{Edd}}$ largely (but not completely) independent of ϵ , and reproducing the observed $\log M_{\text{PEAK}}$ implies $\lambda \approx 0.4 - 0.5$ over the range $0.05 \lesssim \epsilon \lesssim 0.13$.

The higher ρ_\bullet implied by the Hopkins et al. (2007b) local mass function requires a lower efficiency, $\epsilon \approx 0.06$ which in turn implies a higher $\dot{m}_0 \approx 1$ to match $\log M_{\text{PEAK}}$. (Note that this is *not* the comparison in Figure 8d, where we use the HRH07 luminosity function but show our standard estimate of the local mass function). Our inferred ranges for ϵ and \dot{m}_0 are consistent with the findings of Marconi et al. (2004) and S04, who obtained $(\epsilon, \lambda) = (0.08, 0.5)$ and $(0.09, 0.3)$, respectively. Note that S04 tends towards slightly higher values of the radiative efficiency mainly because they used an X-ray bolometric correction normalized to the optical bolometric correction of Elvis et al. (1994), i.e., $C_B = 11.8$, while we have adopted the lower value suggested by recent work (see § 2).

With ϵ and \dot{m}_0 fixed by matching ρ_\bullet and $\log M_{\text{PEAK}}$, there is no freedom in the model to adjust the predicted width and asymmetry of the mass function, but these prove remarkably insensitive to ϵ and \dot{m}_0 in any case. To substantially alter these predictions one must either change the input luminosity function or add a new physical ingredient to the model, such as mass- or redshift-dependent \dot{m}_0 , mergers, or multiple accretion rates. For our minimal model and standard LF estimate, the predicted widths are larger than any of the observational estimates. This discrepancy is largely a consequence of the shallow high-mass slope of the predicted mass function (see Figure 8), which in turn is sensitive to the bright-end slope of the luminosity function in the range $1 \lesssim z \lesssim 3$, as discussed earlier. Note, however, that the observational estimates of $(\Delta \log M_\bullet)_{1/2}$ depend on the extrapolation of the black hole-galaxy correlations above $M_\bullet \approx 10^9 M_\odot$, where they are quite uncertain, so the grey band in Figure 9 should not necessarily be taken as a true upper limit. The predicted asymmetries are in reasonable agreement with the observational estimates, except for the Graham et al. (2007) mass function, in which the population of low mass black holes is greatly reduced.

³ Our reference model of § 4.2 has ϵ at the low end of this range, rather than the middle, because we chose parameters to match the mass function near its peak, where it is best determined. However, the reference model predicts $\rho_\bullet = 5.24 \times 10^5 M_\odot \text{Mpc}^{-3}$, above the middle of the grey band.

Figure 10 presents a similar comparison for models with different input luminosity functions. Here we fix $\dot{m}_0 = 0.75$ in all cases, noting that the value of \dot{m}_0 affects the predicted $\log M_{\text{PEAK}}$ but has little impact on other quantities. Eliminating Compton-thick sources from our standard LF (dotted curve) lowers the efficiency required to match a given ρ_\bullet by about 20%, to $\epsilon = 0.062$ for $\rho_\bullet = 4.26 \times 10^5 M_\odot \text{Mpc}^{-3}$ (short-dashed line). Doubling the Compton-thick contribution (not shown) has a similar effect in the opposite direction, raising the required ϵ by 20%. Changing the Compton-thick contribution has little impact on $\log M_{\text{PEAK}}$ for a given ϵ , or on the width or asymmetry of the predicted mass function. Eliminating *all* obscured sources and retaining only Type I quasars drastically reduces the predicted ρ_\bullet , so such a model (which is implausible on direct observational grounds anyway) can only be reconciled with the local black hole population if the efficiency is very low or if the true value of ρ_\bullet is significantly below our observational estimate. However, a model in which the full bolometric luminosity function is just three times that of Type I AGN — two obscured sources for every unobscured source independent of luminosity and redshift — yields similar predictions to our full model with the luminosity-dependent column density distribution of U03.

For the HRH07 luminosity function, we require $0.079 \lesssim \epsilon \lesssim 0.125$ to reproduce the grey-band range of ρ_\bullet , 25% higher than our standard LF at fixed ρ_\bullet . As discussed earlier, this difference mainly reflects the higher bolometric correction adopted by HRH07, which boosts the normalization of the LF at intermediate redshifts. The HRH07 LF also leads to a higher M_{PEAK} at a given ϵ , and matching $\log M_{\text{PEAK}}/M_\odot \approx 8.5$ implies $0.7 \lesssim \dot{m}_0 \lesssim 1.1$ for the range of ϵ that matches ρ_\bullet . The HRH07 LF predicts a somewhat narrower and more asymmetric mass function, mainly because of the steeper bright-end slope at intermediate redshifts, which steepens the high mass end of the black hole mass function. These results accord with those shown already in Figure 8d. If we adopt *both* the HRH07 luminosity function and the Hopkins et al. (2007b) black hole mass function, which has $\rho_\bullet = 5.7 \times 10^5 M_\odot \text{Mpc}^{-3}$ and $\log M_{\text{PEAK}}/M_\odot \approx 8.4$, we find $\epsilon = 0.075$ and $\dot{m}_0 = 1.3$.

The remaining uncertainties in the luminosity function and the local black hole mass function still leave considerable uncertainty in the radiative efficiency. If we assume that our no-Compton-thick LF and the HRH07 LF bracket the luminosity function uncertainty and our grey band brackets the ρ_\bullet uncertainty, the allowed range is $0.05 \lesssim \epsilon \lesssim 0.125$, and there is clearly some room for the luminosity function or ρ_\bullet to be outside this range. However, the high efficiencies predicted by MHD simulations of thick accretion disks around rapidly spinning black holes, $\epsilon \approx 0.15 - 0.2$ (e.g., Gammie et al. 2004), can only represent the mean efficiency of black hole accretion if ρ_\bullet is considerably below our estimates or the luminosity function is substantially higher than even the HRH07 estimate. There are some ρ_\bullet estimates as low as $2 - 3 \times 10^5 M_\odot \text{Mpc}^{-3}$ (e.g., Wyithe et al. 2004). Our conclusions about efficiency are in agreement with most previous studies, though Elvis et al. (2002) reached a different conclusion mainly because they assumed that the sources producing the X-ray background have an effective mean redshift of $z \sim 2$, while subsequent data have shown that the peak contribution to the background is at $z \lesssim 1$ (e.g., U03; La Franca et al. 2005).

4.4. Redshift-dependent Eddington ratio

So far we have assumed that all black holes at all times radiate at a constant, mildly sub-Eddington rate, an assumption supported by Kollmeier et al. (2005)’s results for luminous quasars in the AGES survey at $0.5 \lesssim z \lesssim 4$. However, Eddington ratios of local AGN have a wide distribution, with a large fraction of Seyferts radiating at $\lambda < 0.1$. Some studies also show evidence for mass-dependence of the typical Eddington ratio (e.g., Heckmann et al. 2004; Vestergaard 2004; McLure & Dunlop 2004; Constantin & Vogeley 2006; Dasyra et al. 2007; Shen et al. 2007b), though systematic uncertainties in the reverberation mapping techniques and extrapolations of empirical virial relations (e.g., Kaspi et al. 2000; Bentz et al. 2006) make it hard to draw firm conclusions. In this section and the one that follows, we discuss simple models with \dot{m}_0 values (and thus Eddington ratios) that depend on redshift or mass. More realistic models would incorporate a *range* of Eddington ratios with the relative importance of high and low accretion rates depending on mass or redshift; we will investigate such models in future work. We note again that the integrated black hole mass density should depend only on ϵ (equation 4), but the shape of the black hole mass function can change if \dot{m}_0 is not constant.

Figure 11 compares the results of our reference model, which has $\epsilon = 0.065$, $\dot{m}_0 = 0.6$, to a model with the same ϵ but

$$\dot{m}_0(z) = [1 - \exp(-z/z_s)], \quad (17)$$

with $z_s = 2$. This implies values of $\dot{m}_0 = 0.78, 0.63, 0.39, 0.22, 0.095, 0.049$ at $z = 3, 2, 1, 0.5, 0.2, 0.1$, respectively, which are consistent with the average drop shown in Figure 6b of Vestergaard et al. (2004) for the more massive black holes, assuming the distribution starts at $\dot{m}_0 \approx 1$ at very high redshifts. The decreasing $\dot{m}_0(z)$ significantly alters the shape of the black hole mass function (Figure 11a) by shifting the low redshift growth of the mass density away from low mass black holes and towards higher mass black holes. This model still requires a substantial number of low-mass black holes residing in spiral galaxy bulges if it is to match the local mass function.

Figure 11b compares the duty cycles produced by the $\dot{m}_0(z)$ model to those from the reference model, at several redshifts. The reference model duty cycles are strongly decreasing functions of redshift and black hole mass, dropping by up to two orders of magnitude in the lower redshift bins. The $\dot{m}_0(z)$ -model “damps” the downsizing, leaving a much milder variation of the duty cycle over time and mass. As emphasized by SW03, the downward shift of the LF break luminosity at $z < 2$ can be explained either by a strong suppression of activity in high mass black holes or by a drop in characteristic Eddington ratios. Our $\dot{m}_0(z)$ model is a compromise between these two explanations; higher mass black holes still build their mass earlier than low mass black holes, but the difference is smaller than in the reference model (Figure 11c).

Greene & Ho (2007) have recently estimated the local MF for active black holes through the virial relations mentioned above. When compared with the local mass function of relic black holes, their study supports a duty-cycle of $P_0 \sim 10^{-2.35}$ for black holes with mass $\log M_\bullet / M_\odot \gtrsim 7$, consistent with the $z \sim 0$ duty-cycle inferred from this model, and about two orders of magnitude above the one corresponding to our reference model (Figure 11b).

4.5. Eddington ratio varying with black hole mass

In the previous section we studied a model in which the Eddington ratio steadily decreases with redshift and is fixed with black hole mass. Here we consider the complementary model in which the Eddington ratio distribution is constant with redshift but declines with black hole mass.

We adopt

$$\dot{m}_0(M_\bullet) = 0.445 \times \left(\frac{M_\bullet}{10^9 M_\odot} \right)^{0.5} \quad (18)$$

with a constant radiative efficiency $\epsilon = 0.075$. As discussed in § 4.1, we evolve this model by integrating equation (15) with a fixed black hole mass grid, extrapolating the luminosity function below $L_{\text{MIN}}(z)$. Relative to the reference model, the $\dot{m}_0(M_\bullet)$ model associates the peak of the LF with higher mass black holes, especially at lower redshifts. The low redshift growth of low mass black holes is strongly suppressed, and the $z = 0$ abundance of low mass black holes is much lower, consistent with the Graham et al. (2007) local mass function estimate, as shown in Figure 12. The dependence of duty cycle on mass is also much stronger in this model because of the paucity of low mass black holes; note that the duty cycle at low masses is high but the amount of growth is low because of the low accretion rates. Getting our mass-dependent \dot{m}_0 model to run at all requires a high initial black hole density, with a duty cycle $P_0(z = 6) = 0.01 - 0.02$; otherwise, the slow growth of low mass black holes leads to required duty cycles that exceed unity at intermediate redshifts. Alternatively, we can start with a higher initial duty cycle and only “turn on” the mass dependence of equation (18) after an epoch of growth at constant \dot{m}_0 .

More generally, we can vary the Eddington ratio both in redshift and mass, $\dot{m}_0(M_\bullet, z) = T(z)B(M_\bullet)$. The continuity equation can then be written

$$\begin{aligned} \frac{\partial n(M_\bullet, t)}{\partial t} &= - \frac{T(z)}{(\ln 10)^2 M_\bullet} \times \quad (19) \\ \frac{\partial}{\partial \log M_\bullet} \left[B(M_\bullet) \Phi(L, z) \left| \frac{d \log L}{d \log M_\bullet} \right| \right] &= - \frac{T(z)}{\ln(10)^2 M_\bullet} \times \\ \left[B(M_\bullet) \frac{\partial \Phi(L, z)}{\partial \log L} \left(\frac{\partial \log L}{\partial \log M_\bullet} \right)^2 + \left| \frac{\partial \log L}{\partial \log M_\bullet} \right| \Phi(L, z) \frac{\partial B(M_\bullet)}{\partial \log M_\bullet} \right], \end{aligned}$$

where we have set to zero the *second* derivative $\partial^2 \log L / (\partial \log M_\bullet)^2$ assuming a power-law relation like that in equation (18). We have used equation (19) to investigate models in which we vary the Eddington ratio with redshift and mass as given in equations (17) and (18). We find that we can get somewhat better fits to Graham et al.’s (2007) local mass function, since both the implemented trends act to decrease the numbers of low mass black holes.

4.6. Black hole mergers

Observations show, and hierarchical galaxy formation models predict, that a significant fraction of galaxies experience mergers with comparably massive galaxies during their lifetime. At least some of these galaxy mergers are likely to be accompanied by mergers of the central black holes that they contain, though the mechanisms that shrink black hole orbits to the scale where gravitational radiation can drive a final merger are not fully understood (see Merritt & Milosavljević 2005). In a future paper, we will combine our accretion model with theoretically predicted merger rates for cold dark matter subhalos (Yoo et al. 2007) to create models with realistic contributions of accretion and merger driven

growth. Here we illustrate the potential impact of mergers on the black hole mass function using a simple mathematical model that assumes constant probability of equal mass mergers per Hubble time, similar to the models of Richstone et al. (1998) and SW03. We will ignore physically interesting complications such as ejection of black holes by gravitational radiation or three-body interactions or variations of radiative efficiency caused by the impact of mergers on the black hole spin distribution (e.g., Hughes & Blandford 2003; Volonteri et al. 2003; Gammie et al. 2004; Islam et al. 2004; Yoo & Miralda-Escudé 2004; Merritt & Milosavljević 2005; Volonteri et al. 2006). These effects, along with unequal mergers and the mass and redshift-dependence of merger rates, should be considered in a complete model of the evolving black hole population. Mergers redistribute mass within the black hole population, but they do not change the integrated mass density, so they do not affect the integrated Softan (1982) argument. (In principle, gravitational radiation during mergers can *reduce* the integrated mass density [see Yu & Tremaine 2002], but we do not consider this effect here).

In our model, a black hole of mass M_\bullet has a probability P_{merg} of merging with an equal mass black hole in the Hubble time $t_H(z)$ (age of the Universe at redshift z). Therefore the fraction F of black holes that merge in a timestep Δt is

$$F = P_{\text{merg}} \times \frac{\Delta t}{t_H(z)}. \quad (20)$$

At each time t_1 , we first advance the mass function to time $t_2 = t_1 + \Delta t$ with accretion only, then add to each bin of the mass function an increment (which may be positive or negative)

$$\Delta\Phi(M_\bullet, t_2) = \frac{F \times \Phi(\frac{M_\bullet}{2}, t_2)}{2} - F \times \Phi(M_\bullet, t_2), \quad (21)$$

where the second term represents black holes lost from the bin by merging and $\Phi(\frac{M_\bullet}{2}, t_2)$ is calculated by interpolation.

Figure 13 shows the evolution of the black hole mass function for a model with $P_{\text{merg}} = 0.5$ and our reference model values of $\epsilon = 0.065$ and $\dot{m}_0 = 0.6$. Comparing the $z = 0.02$ output to that of the reference model shows that the net effect of merging is to slightly lower the abundance of black holes below the peak of the mass function and to significantly increase the abundance of very massive black holes, as expected (see also Malbon et al. 2006; Yoo et al. 2007). Although we start merging at $z = 6$, comparison of Figure 13 to Figure 7b shows that the mass function is nearly identical to that of the reference model down to $z = 1$. Mergers at this level only change the mass function noticeably once accretion-driven evolution has slowed.

Since our reference model already produces an excess of massive black holes relative to local estimates of the black hole function, adding mergers only makes the match to observations worse. However, the impact of mergers is evident mainly at $M_\bullet > 10^9 M_\odot$, where the local mass function estimates are most sensitive to the adopted scatter in the black hole-host scaling relations and to the extrapolations of these relations to the most luminous galaxies. Accommodating the predictions of our merger model would require an intrinsic scatter of ~ 0.5 dex at high masses, or a change in slope of the scaling relations. Either of these changes seems possible given the current observational uncertainties, but neither seems likely (see, e.g., discussions by Wyithe 2004; Batchelder et al. 2006; Lauer et al. 2006; Tundo et al. 2007). If we adopt the HRH07 LF in place of our standard LF, then the predicted black hole mass function *with* mergers is similar to that

of our reference model *without* mergers (see Figure 13). The impact of mergers at this level is therefore comparable to the systematic uncertainties associated with the AGN luminosity function.

In fact, the value $P_{\text{merg}} = 0.5$ is high compared to theoretical predictions for massive galaxies (Maller et al. 2006), and theoretically predicted merger rates decline towards lower masses. Observational estimates of the galaxy merger rate and its mass dependence span a substantial range (see, e.g., Bell et al. 2006; Conroy et al. 2007; Masjedi et al. 2008, and references therein), and $P_{\text{merg}} = 0.5$ is roughly consistent with the high end of these estimates. We conclude that the impact of mergers on the black hole mass function is probably small compared to remaining uncertainties in accretion-driven growth, except perhaps for the rare, high mass black holes. The most interesting impact of black hole mergers may arise indirectly, through their effect on black hole spins and thus on radiative efficiencies (e.g., Volonteri et al. 2005).

4.7. Tabulation of luminosity and mass functions

For the convenience of readers who may wish to use them, we provide electronic tables that list our estimate of the AGN bolometric LF and some of our model predictions of the black hole mass function and duty cycle, all as a function of redshift. Table 2 lists our standard LF estimate, the LF after eliminating or doubling the number of Compton thick sources, and the HRH07 LF estimate evaluated at the same redshifts and luminosities for convenient comparison. Table 3 lists the predicted black hole mass function at the same redshifts for our reference model values of $\epsilon = 0.065$, $\dot{m}_0 = 0.60$, computed for each of the luminosity functions in Table 2. The final column lists the mass function predicted for the HRH07 LF and the parameter values $\epsilon = 0.09$ and $\dot{m}_0 = 1$, which yield a good match to the local mass function for this LF. Table 4 lists instead the duty cycles corresponding to the same models reported in Table 3, computed at the same redshifts and black hole masses. [Prior to publication, the full tables can be found in electronic format at <http://www.astronomy.ohio-state.edu/~shankar/Models/>]

5. SPACE DENSITY AND BIAS OF AGN HOSTS

Predictions of the black hole mass function at redshifts $z > 0$ can be tested observationally if one assumes that black hole mass increases monotonically with the luminosity of the host galaxy or the mass of its parent halo. This assumption is unlikely to be perfect, but given the tight correlation between black hole mass and bulge mass observed today, it may be a reasonable approximation. Figure 14a shows, at several redshifts, the predictions of our reference model for the cumulative space density of galaxies that can host an AGN of luminosity L or greater. Since the model assumes a single \dot{m}_0 , this is simply equal to the cumulative space density of black holes of mass $M_\bullet > L/(f_{0.1}\dot{m}_0 l) = 1.9 \times 10^8 M_\odot \times (L/10^{46} \text{ erg s}^{-1})$. If the monotonic assumption holds, then the observed space density of galaxies brighter than $L_{\text{host}}(L_{\text{AGN}})$ should equal the space density predicted in Figure 14a, where $L_{\text{host}}(L_{\text{AGN}})$ is the luminosity of galaxies that host AGN of luminosity L_{AGN} .

As emphasized by Haiman & Hui (2001) and Martini & Weinberg (2001), the clustering of AGN can be a powerful diagnostic for the duty cycle of black hole activity: a high duty cycle implies that halos of AGN are rare, hence high mass, hence strongly clustered. In the context of our models, we can predict the halo mass M_h associated with black holes

of mass M_\bullet by matching the cumulative mass functions,

$$\Phi(> M_\bullet, z) = \Phi(> M_h, z). \quad (22)$$

Here $\Phi(> M_\bullet, z)$ is the space density of black holes more massive than M_\bullet at redshift z , in units of Mpc^{-3} , as predicted by our evolutionary model, and $\Phi(> M_h, z)$ is the space density of halos more massive than M_h expected for a ΛCDM cosmological model, which we compute using the Sheth & Tormen (1999) halo mass function with cosmological parameters $\Omega_m = 0.3, \Omega_\Lambda = 0.7, h = 0.7, \sigma_8 = 0.8$ and linear power spectrum taken from Smith et al. (2003) with $\Gamma = 0.2$. This determination assumes both a monotonic relation between black hole mass and halo mass and one black hole per halo, but we have checked that allowing black holes to reside in subhalos does not substantially change our results if we adopt the subhalo statistics of Vale & Ostriker (2004). Finally, we compute the bias of black holes of mass M_\bullet , and thus the bias of AGN of luminosity $L = f_{0.1} \dot{m}_0 / M_\bullet$, using Sheth et al.'s (2001) analytic model for halo bias,

$$b(L, z) = b(M_\bullet, z) = b(M_h, z). \quad (23)$$

Figure 14b shows the predicted bias as a function of luminosity L at several redshifts for the reference model of § 4.2. The predicted bias is much stronger at high redshift because the comoving space density of black holes is lower (Figure 7) and because the bias of halos of a given space density is higher. Points in Figure 14b show recent observational estimates of AGN clustering bias from the 2dF and SDSS quasar redshift surveys (da Angela et al. 2007; Myers et al. 2007; Porciani & Norberg 2007) in the redshift range $0.8 \lesssim z \lesssim 1.3$ and $1.7 \lesssim z \lesssim 2.1$ (Porciani & Norberg 2007) and from SDSS at $3 \lesssim z \lesssim 3.5$ (Shen et al. 2007a). Our reference model is quite successful at predicting the absolute level of bias (and thus AGN clustering strength) for quasars with $L \geq 10^{46} \text{ erg s}^{-1}$ at $z \sim 1$, $z \sim 2$ and $z \sim 3$, and, especially, at explaining the strong trend of bias among these samples. It appears to underpredict the clustering of lower luminosity AGN at $z \sim 1$, though Myers et al. (2007) note the including the possible impact of stellar contamination on their sample expands their error bars by a factor of ~ 1.5 (an effect we have not included in Figure 14b).

We reserve a detailed examination of AGN clustering constraints — including an assessment of what models can be ruled out with present data or improved measurements — for future work. Allowing scatter between black hole mass and halo mass or a range of Eddington ratios can significantly alter predictions both for AGN host density and for AGN clustering, so these classes of models will be especially interesting to explore. For example, the stronger clustering in the Myers et al. (2007) sample relative to our reference model predictions could indicate that a fraction of these lower luminosity AGN are associated with high mass black holes radiating at low Eddington ratios (e.g., Lidz et al. 2006).

6. DISCUSSION

We have constructed self-consistent models for the evolution of the supermassive black hole population and the AGN population, in which black holes grow at the rate implied by the observed luminosity function given assumed values of the radiative efficiency ϵ and the characteristic accretion rate $\dot{m}_0 = \dot{M}_\bullet / \dot{M}_{\text{Edd}}$ (see Eqs. 10, 12, 15). These models can be tested against the mass distribution of black holes in the local universe, and they make predictions for the duty cycles of black holes as a function of redshift and mass, which

can be tested against observations of quasar hosts and quasar clustering if one assumes an approximately monotonic relation between the masses of black holes and the masses of their host galaxies and halos. Our method is similar to that used previously by Cavaliere et al. (1971), Small & Blandford (1992), Yu & Tremaine (2002), SW03, Marconi et al. (2004), and S04. However, we have drawn on more recent data on the AGN luminosity function and the local black hole mass function, and we have considered a broader spectrum of models. This approach can be considered a “differential” generalization of the Sołtan (1982) argument relating the integrated emissivity of the quasar population to the integrated mass density of the local black hole population.

Our model for the bolometric AGN luminosity function starts from the model of U03, based on X-ray data from a variety of surveys, but we adjust its parameters as a function of redshift in light of more recent measurements and data at other wavelengths. In agreement with previous studies we find that the LF of optical AGNs is roughly consistent with that of X-ray AGN that have absorbing column densities $\log N_H / \text{cm}^{-2} \leq 22$ and that unobscured AGN dominate the bright end of the LF. We show that the latest constraints on the hard X-ray background ($E \sim 10 - 100 \text{ keV}$) from *INTEGRAL* and from the *PDS* instrument on BeppoSax support a reduced normalization relative to extrapolations from other missions at lower energies. They therefore favor a lower contribution from very highly obscured AGN ($\log N_H / \text{cm}^{-2} \gtrsim 24.5$) than some previous estimates (but see also Gilli et al. 2007). Our estimate of the bolometric AGN LF is independent in implementation but similar in spirit to that of HRH07. The most significant differences for purposes of this investigation are that HRH07 have a higher LF normalization at $z \sim 1 - 3$, principally because of their choice of bolometric correction, and they have a steeper bright-end slope at $z \sim 1 - 2.5$, where they adopt the slopes measured by Richards et al. (2006) from the SDSS and we use the slopes inferred by U03 from X-ray data. We regard the differences between our estimate and that of HRH07 as a reasonable indication of the remaining systematic uncertainties in the bolometric LF of AGNs.

With our LF estimate, the bolometric emissivity of the AGN population tracks recent estimates of the cosmic star formation rate as a function of redshift. (Comparisons based on the space density of high luminosity quasars [e.g., Richards et al. 2006, Osmer 2004 and references therein] reach a different conclusion because at low redshifts the bright end of the AGN LF drops much more rapidly with time than the overall emissivity.) The integrated black hole mass density implied by this emissivity is $\sim 8 \times 10^{-4}$ of the stellar mass at all redshifts, or about half of the estimated ratio of black hole mass to bulge stellar mass in local galaxies. This tracking favors scenarios in which black holes and the stellar mass of bulges grow in parallel, with about 50% of the star formation linked to black hole growth at all redshifts. These findings are hard to reconcile with any models where black hole growth substantially precedes stellar mass buildup, or with recent claims that the ratio of black hole mass to stellar mass is much larger at high redshift than the local value. However, our finding refers to integrated densities, so it does not indicate the relative timing of black hole and bulge growth on an object-by-object basis.

Observational estimates of the local black hole mass function still show substantial discrepancies among different authors, depending on the correlation used to derive it (e.g., $M_\bullet - \sigma$, $M_\bullet - L_{\text{bulge}}$, $M_\bullet - M_{\text{star}}$, M_\bullet -Sérsic index, or fundamental plane), the calibration of the correlation, and the intrinsic

sic scatter of the correlation. Above $M_\bullet \sim 10^9 M_\odot$, estimates depend on extrapolation of the observed scaling relations, and below $M_\bullet \sim 10^{7.5} M_\odot$ they are sensitive to the treatment of spiral bulges. The grey band in Figure 5 (and subsequent figures) encompasses most estimates, but the fundamental plane (Hopkins et al. 2007b) and Sérsic index (Graham et al. 2007) methods imply more sharply peaked mass functions. The integrated mass densities of all of these estimates are in the range $\rho_\bullet \sim 3 - 5.5 \times 10^5 M_\odot \text{Mpc}^{-3}$.

Our simplest models assume a single characteristic Eddington accretion rate \dot{m}_0 , independent of redshift and black hole mass, and all of our models assume a single value of the radiative efficiency ϵ . Matching the local black hole mass density requires $\epsilon = 0.075 \times (\rho_\bullet / 4.5 \times 10^5 M_\odot \text{Mpc}^{-3})^{-1}$ for our standard estimate of the AGN LF, or $\epsilon \sim 0.094 (\rho_\bullet / 4.5 \times 10^5 M_\odot \text{Mpc}^{-3})^{-1}$ for the HRH07 luminosity function.⁴ With ϵ thus fixed, the value of \dot{m}_0 determines the peak of the predicted local black hole mass function in the $M_\bullet \Phi(M_\bullet)$ vs M_\bullet plane. Note that with our definitions the Eddington luminosity ratio is $\lambda = L/L_{\text{Edd}} \approx \dot{m}_0 (\epsilon/0.1)$ (equation 9). Matching the observed peak at $\log M_\bullet / M_\odot \sim 8.5$ implies $\dot{m}_0 \approx 0.6$ ($\lambda \approx 0.45$) for our standard LF estimate and $\dot{m}_0 \approx 1$ ($\lambda \approx 0.95$) for the HRH07 LF. Lower values, $\dot{m}_0 = 0.1 - 0.3$, shift the peak location to untenably high masses, $\log M_\bullet / M_\odot \sim 8.9 - 9.3$ or, for HRH07, $\log M_\bullet / M_\odot \sim 9.1 - 9.6$. The single- \dot{m}_0 models achieve a reasonable match to our “grey-band” observational estimates of the width and asymmetry of the local mass function, though for our LF estimate the predicted mass function is too high at $M_\bullet > 10^9 M_\odot$ and is therefore somewhat too broad. Single- \dot{m}_0 models cannot reproduce the more sharply peaked local mass functions estimated by Graham et al. (2007) or Hopkins et al. (2007b).

Our reference model, which has $\epsilon = 0.065$, $\dot{m}_0 = 0.60$, and our standard LF estimate, predicts a duty cycle for activity of $10^9 M_\odot$ black holes that declines steadily from 0.15 at $z = 4$ to 0.07 ($z = 3$), 0.035 ($z = 2$), 0.004 ($z = 1$), and 10^{-4} ($z = 0$). The decline in duty cycle for lower mass black holes is much shallower. Massive black holes therefore build their mass relatively early while low mass black holes grow later, the phenomenon often referred to as “downsizing”. Our results on mean radiative efficiency and duty cycle evolution are also in qualitative agreement with those found by Haiman et al. (2004). The predicted duty cycles seem in reasonable accord with observational estimates, though these estimates have considerable uncertainty and do not, as yet, probe mass and redshift dependence in much detail. The electronic tables described in § 4.7 provide tabulations as a function of redshift of our AGN bolometric LF estimate, the HRH07 LF, and black hole mass functions and duty cycles for single- \dot{m}_0 models that are in good agreement with the observed $z = 0$ mass functions given these LF inputs.

We have examined models in which the Eddington ratio accretion rate \dot{m}_0 is reduced at low redshift or at low black hole mass. Declining redshift evolution of \dot{m}_0 damps “downsizing,” reducing the dependence of duty cycles on black hole mass and redshift. This model produces a typical duty cycle $P_0 \sim 10^{-2.5}$ at $z = 0$, about two orders of magnitude higher than in the reference model and consistent with the local duty cycle inferred from observations by Greene & Ho (2007). In general terms, the observed luminosity-dependent density evolution of the AGN LF can be explained by preferential sup-

pression of activity in high mass black holes at low redshift, by a decline in the typical accretion rate at low redshift, or by some combination thereof. The mass-dependent \dot{m}_0 model associates more of the AGN emissivity to high mass black holes, so it predicts a $z = 0$ mass function that is more sharply peaked, in better agreement with the estimates of Hopkins et al. (2007b) and Graham et al. (2007) but worse agreement with other estimates. This model predicts a stronger mass dependence of duty cycles than our reference model because it maps low mass black holes, whose abundance is already suppressed, to less luminous, and hence more common, AGN.

We have also considered a model in which each black hole has a 50% probability per Hubble time of merging with another black hole of equal mass. Merger-driven growth in this model has little impact on the black hole mass function until $z < 1$, when accretion-driven evolution has slowed. Low redshift mergers slightly depress the low mass end of the $z = 0$ mass function and significantly enhance the high mass tail, worsening the agreement with observational estimates. Models incorporating theoretically predicted merger rates can allow more realistic calculations of the impact of mergers on the black hole population; this impact will probably be smaller than in the simplified model considered here.

We have calculated the clustering bias of AGN as a function of luminosity and redshift for our reference model, assuming a monotonic relation between black hole mass and halo mass. The predictions are in reasonable accord with observational estimates. We will examine AGN clustering predictions in more detail in future work, with attention to what models can be excluded by the data and what can be learned by matching the full AGN correlation function in addition to an overall bias factor.

MHD simulations (e.g., Gammie et al. 2004; Shapiro 2005) show that disk accretion onto Kerr black holes spins them up to an equilibrium spin rate $a \approx 0.95$ (where $a = 1$ is the angular momentum parameter for a maximally rotating black hole). The radiative efficiency in these models is $\epsilon \approx 0.16 - 0.2$. These high efficiencies would lead to black hole mass densities a factor of two or more below our central estimate, and below our estimated lower bound. Furthermore, our results show that models with ϵ in the range 0.06 – 0.11 can achieve a good match to the overall shape of the black hole mass function near the peak in $M_\bullet \Phi(M_\bullet)$, not just the value of ρ_\bullet , given plausible choices of \dot{m}_0 . Systematic uncertainties in the AGN LF do not appear large enough to accommodate $\epsilon \gtrsim 0.15$. Accommodating these high efficiencies would instead require a substantial downward revision of recent estimates of the local black hole mass function, reducing the integrated mass density to $\rho_\bullet \sim 2 \times 10^5 M_\odot \text{Mpc}^{-3}$. Our results are consistent with a scenario like the one of King & Pringle (2006) in which chaotic accretion spins down black holes because of counter-alignment with the accretion disk angular momentum, or with other mechanisms that reduce efficiencies below the MHD-simulation predictions.

The assumption that all active black holes at a given mass and redshift have the same \dot{m}_0 is clearly an idealization, at least in the local universe where observations indicate a wide range of Eddington ratios (Heckman et al. 2005; Greene & Ho 2007). Steed & Weinberg (2003) and Yu & Lu (2004) discussed continuity equation models evolved adopting a distribution of Eddington ratios. In particular, Yu & Lu (2004) have derived the relation between the integrated number of AGNs shining at all times at a given luminosity L , the mean light curve of black holes, and the local black hole mass func-

⁴ More precisely, it is $\epsilon/(1 - \epsilon)$ that is proportional to ρ_\bullet^{-1} , but the difference from $\epsilon \propto \rho_\bullet^{-1}$ is tiny over the allowed range.

tion. Following their equation (18), we find that a good match between the cumulative number of AGNs and of relic black holes can be achieved for $\epsilon \sim 0.07$ (required by the Softan argument) and a mean AGN light curve exponentially increasing with $\lambda = 0.6$ and a negligible declining phase, similar to our reference model. Alternatively, we find that a good match can be obtained by assuming that black holes grow rapidly in a Super-Eddington phase with $\lambda \gtrsim 2$ and then have a long declining phase, qualitatively resembling our $\dot{m}(z)$ model discussed in § 4.4. In future work we will investigate models that incorporate multiple \dot{m}_0 -values and accretion modes, including the addition of modest log-normal scatter in $\dot{m}_0(M, z)$ (e.g., Kollmeier et al. 2005; Netzer et al. 2007; Shen et al. 2007b) and sharper revisions in which some black holes accrete at super-Eddington or highly sub-Eddington rates, perhaps with reduced radiative efficiencies (Narayan, Mahadevan, & Quataert 1998 and references therein). We will also incorporate mergers at the rates predicted by theoretical models of cold dark matter subhalos and their associated black

holes (Yoo et al. 2007). For appropriate parameter choices, we expect that many scenarios can be made consistent with the observed AGN LF and the local black hole mass function. However, direct measurements of Eddington ratio distributions and measurements of AGN clustering and host properties, all as a function of luminosity and redshift, should greatly narrow the field of viable models. Within the (often substantial) uncertainties of existing data, a simple model in which all black holes grow by accreting gas at mildly sub-Eddington rates with a radiative efficiency $\epsilon \approx 0.06 - 0.1$ is surprisingly successful at reproducing a wide range of observations.

This work was supported by NASA grant GRT000001640 and by Spanish ministry grants AYA2006-06341 and AYA2006-15623-C02-01. We thank Alister Graham and Philip Hopkins for providing data on their results on the local black hole mass function and John Silverman for providing data on the X-ray luminosity function.

REFERENCES

- Alexander, D. M., et al. 2003, *AJ*, 126, 539
 Antonucci, R. R. 1993, *ARA&A*, 31, 473
 Babic, A., Miller, L., Jarvis, M. J., Turner, T. J., Alexander, D. M., & Croom, S. M. 2007, *A&A*, 474, 755
 Ballantyne, D. R., & Papovich, C. 2007, *ApJ*, 660, 988
 Barger, A. J., Cowie, L. L., Capak, P., Alexander, D. M., Bauer, F. E., Brandt, W. N., Garmire, G. P. & Hornschemeier, A. E. 2003, *ApJ*, 584, L61
 Barger, A. J., & Cowie, L. L. 2005, *ApJ*, 635, 115
 Barger, A. J., et al. 2005, *AJ*, 129, 578
 Batcheldor, D., Marconi, A., Merritt, D., & Axon, D. J. 2007, *ApJL*, 663, 85
 Bell, E. F., Phleps, S., Somerville, R. S., Wolf, C., Borch, A., & Meisenheimer, K. 2006, *ApJ*, 652, 270
 Bentz, M. C., Peterson, B. M., Pogge, R. W., Vestergaard, M., & Onken, C. A. 2006, *ApJ*, 644, 133
 Bernardi, M., Sheth, R. K., Tundo, E., & Hyde, J. B. 2007, *ApJ*, 660, 267
 Binney, J., & Merrifield, M. 2000, *Galactic Astronomy*, Princeton Univ. Press
 Bolton, J. S., Haehnelt, M. G., Viel, M., Springel, V. 2005, *MNRAS*, 357, 1178
 Bongiorno, A., et al. 2007, *A&A*, 472, 443
 Borys, C., Smail, I., Chapman, S. C., Blain, A. W., Alexander, D. M., Ivison, R. J. 2005, *ApJ*, 635, 853
 Brown, M. J. I., et al. 2006, *ApJ*, 638, 88
 Bundy, K., et al. *ApJ*, submitted, arXiv/0710.2105
 Caputi, K. I., McLure, R. J., Dunlop, J. S., Cirasuolo, M., & Schael, A. M. 2006, *MNRAS*, 366, 609
 Cavaliere, A., Morrison, P., & Wood, K. 1971, *ApJ*, 170, 223
 Cavaliere, A., & Vittorini, V. 2000, *ApJ*, 543, 599
 Churazov, E., et al. 2007, *A&A*, 467, 529
 Comastri, A., Setti, G., Zamorani, G., & Hasinger, G. 1995, *A&A*, 296, 1
 Comastri, A. 2004, Review for "Supermassive Black Holes in the Distant Universe", Ed. A. J. Barger, Kluwer Academic, astro-ph/0403693
 Conroy, C., Ho, S., & White, M. 2007, *MNRAS*, 379, 1491
 Constantin, A., & Vogeley, M. S. 2006, 650, 727
 Cool, R. J., Kochanek, C. S., Eisenstein, D. J., Stern, D., Brand, K., Brown, M. J. I., Dey, A., Eisenhardt, P. R., Fan, X., Gonzalez, A. H., Green, R. F., Jannuzi, B. T., McKenzie, E. H., Rieke, G. H., Rieke, M., Soifer, B. T., Spinrad, H., & Elston, R. J. 2006, *AJ*, 132, 823
 Cowie, L. L., et al. 2002, *ApJ*, 566, L5
 Cowie, L. L., et al. 2003, *ApJ*, 584, L57
 Croom, S. M., et al. 2004, *MNRAS*, 349, 1397
 Croton, D. J., Springel, V., White, S. D. M., De Lucia, G., Frenk, C. S., Gao, L., Jenkins, A., Kauffmann, G., Navarro, J. F., & Yoshida, N. 2006, *MNRAS*, 365, 11
 Croton, D. J. 2006b, *MNRAS*, 369, 1808
 da Angela, J., et al. 2006, *MNRAS*, submitted, astro-ph/0612401
 Dasysa, K. M., Tacconi, L. J., Davies, R. I., Naab, T., Genzel, R., Lutz, D., Sturm, E., Baker, A. J., Veilleux, S., Sanders, D. B., & Burkert, A. 2006, *ApJ*, 651, 835
 Dasysa, K. M., Tacconi, L. J., Davies, R. I., Genzel, R., Lutz, D., Peterson, B. M., Veilleux, S., Baker, A. J., Schweitzer, M., & Sturm, E. 2007, *ApJ*, 657, 102
 De Zotti, G., Shankar, F., Lapi, A., Granato, G. L., Silva, L., Cirasuolo, M., Salucci, P., & Danese, L. 2006, *MmSAIt*, 77, 661
 Elvis, M., Risaliti, G., & Zamorani, G. 2002, *ApJ*, 565, L75
 Fabian, A. C., & Iwasawa, K. 1999, *MNRAS*, 303, 34
 Fan, X., et al. 2001, *AJ*, 121, 54
 Fan, X., et al. 2004, *ApJ*, 128, 515
 Fardal, M. A., Katz, N., Weinberg, D. H., & Davé, R. 2007, *MNRAS*, 379, 985
 Ferrarese, L., & Merritt, D. 2000, *ApJ*, 539, L9
 Ferrarese, L. 2002, Proceedings of the 2nd KIAS Astrophysics Workshop, Seoul, Korea, astro-ph/0203047
 Fioc, M., & Rocca-Volmerange, B. 1997, *A&A*, 326, 950
 Fiore, F., et al. 2003, *A&A*, 409, 79
 Fontana, A., et al. 2006, *A&A*, 459, 745
 Fontanot, F., Cristiani, S., Monaco, P., Nonino, M., Vanzella, E., Brandt, W. N., Grazian, A., & Mao, J. 2007, *A&A*, 461, 39
 Fontanot, F., Monaco, P., Cristiani, S., & Tozzi, P. 2006, *MNRAS*, 373, 1173
 Frontera, F., Orlandini, M., Landi, R., Comastri, A., Fiore, F., Setti, G., Amati, L., Costa, E., Masetti, N., & Palazzi, E. 2007, *ApJ*, 666, 86
 Fukugita, M., Hogan, C. J., & Peebles, P. J. E. 1998, *ApJ*, 503, 518
 Gammie, C. F., Shapiro, S. L., & McKinney, J. C. 2004, *ApJ*, 602, 312
 Gilli, R., Comastri, A., & Hasinger, G. 2006, *A&A*, 463, 79
 Graham, A. W., Erwin, P., Caon, N., & Trujillo, I. 2001, *ApJ*, 563, L11
 Graham, A. W., et al. 2007, *MNRAS*, 378, 198
 Graham, A. W. 2007, *MNRAS*, 379, 711
 Granato, G. L., De Zotti, G., Silva, L., Bressan, A., & Danese, L. 2004, *ApJ*, 600, 580
 Granato, G. L., Silva, L., Lapi, A., Shankar, F., De Zotti, G., Danese, L. 2006, *MNRAS*, 368L, 72
 Greene, J. E., & Ho, L. C. 2006, *ApJ*, 641, 21
 Greene, J. E., & Ho, L. C. 2007, *ApJ*, 667, 131
 Greve, T. R., et al. 2005, *MNRAS*, 359, 1165
 Kennefick, J. D., Djorgovski, S. G., & de Carvalho, R. R. 1995, *AJ*, 110, 2553
 Haiman, Z., Ciotti, L., Ostriker, J. P. 2004, *ApJ*, 606, 763
 Häring, N., & Rix, H. W. 2004, *ApJ*, 604, 89
 Hasinger, G., et al. 2001, *A&A*, 365, 45
 Hasinger, G., Miyaji, T., Schmidt, M. 2005, *A&A*, 441, 417
 Heckman, T. M., Kauffmann, G., Brinchmann, J., Charlot, S., Tremonti, C., & White, S. D. M. 2004, *ApJ*, 613, 109
 Hickox, R. C. et al. 2007, *ApJ*, in press, astro-ph/0708.3678
 Hopkins, A. W., & Beacom, J. F. 2006, 651, 142
 Hopkins, P. F., Hernquist, L., Cox, T. J., Di Matteo, T., Robertson, B., & Springel, V. 2006a, *ApJS*, 163, 1
 Hopkins, P. F., Robertson, B., Krause, E., Hernquist, L., & Cox, T. J. 2006b, *ApJ*, 652, 107
 Hopkins, P. F., Richards, G. T., Hernquist, L. 2007a, *ApJ*, 654, 731 (HRH07)
 Hopkins, P. F., Hernquist, L., Cox, T. J., Robertson, B., & Krause, E. 2007b, *ApJ*, in press, astro-ph/0701351
 Hopkins, P. F., Lidz, A., Hernquist, L., Coil, A. L., Myers, A. D., Cox, T. J., & Spergel, D. 2007c, *ApJ*, 662, 110
 Hosokawa, T. 2004, *ApJ*, 606, 139
 Hughes, S. A., & Blandford, R. D. 2003, *ApJ*, 585, L10

- Hunt, M. P., Steidel, C. C., Adelberger, K. L., & Shapley, A. E. 2004, *ApJ*, 605, 625
- Islam, R. R., Taylor, J. E., & Silk, J. 2004, *MNRAS*, 354, 427
- Jiang, L., et al. 2006, *AJ*, 131, 2788
- Kaspi, S., et al. 2000, *ApJ*, 533, 631
- Kemhavi, A. K., & Narlikar, J. V. 1999, in "Quasars and Active Galactic Nuclei", Cambridge Univ. Press, Cambridge
- King, A. R., & Pringle, J. E. 2006, *MNRAS*, 373, 90
- Kollmeier, J. A., et al. 2006, *ApJ*, 648, 128
- La Franca, F., et al. 2005, *ApJ*, 635, 864
- Lapi, A., Shankar, F., Mao, J., Granato, G. L., Silva, L., De Zotti, G., & Danese, L. 2006, *ApJ*, 650, 42
- Lauer, T. R., Faber, S. M., Richstone, D., Gebhardt, K., Tremaine, S., Postman, M., Dressler, A., Aller, M. C., Filippenko, A. V., Green, R., Ho, L. C., Kormendy, J., Magorrian, J., & Pinkney, J. 2006, *ApJ*, 670, 249
- Lauer, T. R., et al. 2007a, *ApJ*, 662, 808
- Lauer, T. R., Tremaine, S., Richstone, D., & Faber, S. M., 2007b, *ApJ*, 670, 249
- Lawrence, J. K. 1991, *MNRAS*, 252, 586
- Lidz, A., Hopkins, P. F., Cox, T. J., Hernquist, L., & Robertson, B. 2006, *ApJ*, 641, 41
- Mahabal, A., Stern, D., Bogosavljevic, M., Djorgovski, S. G., & Thompson, D. 2005, *ApJ*, 634, L9
- Magorrian, J., et al. 1998, *AJ*, 115, 2285
- Magdziarz, P., & Zdziarski, A. A. 1995, *MNRAS*, 273, 837
- Malbon, R. K., Baugh, C. M., Frenk, C. S., & Lacey, C. G. 2006, *MNRAS*, submitted, *astroph/0607424*
- Maller, A. H., Katz, N., Kereš, D., Davé, R., & Weinberg, D. H. 2006, *ApJ*, 647, 763
- Marconi, A., & Hunt, L. 2003, *ApJL*, 589, L21
- Marconi, A., Risaliti, G., Gilli, R., Hunt, L. K., Maiolino, R., & Salvati, M. 2004, *MNRAS*, 351, 169
- Marshall, F. E., et al. 1980, *ApJ*, 235, 4
- Martinez-Sansigre, A. et al., 2005, *Nature*, 436, 666
- Masjedi, M., Hogg, D. W., & Blanton, M. R. 2008, *ApJ*, 679, 260
- Matt, G., Fabian, A. C., Guainazzi, M., Iwasawa, K., Bassani, L., & Malaguti, G. 2000, *MNRAS*, 318, 173
- McLure, R. J., Dunlop, J. S. 2002, *MNRAS*, 331, 795
- McLure, R. J., Dunlop, J. S. 2004, *MNRAS*, 352, 1390
- McLure, R. J., Jarvis, M. J., Targett, T. A., Dunlop, J. S., & Best, P. N. 2006, *MNRAS*, 368, 1359
- Merloni, A. 2004, *MNRAS*, 353, 1035
- Merloni, A., Rudnick, G., & Di Matteo, T. 2004, *MNRAS*, 354, 37
- Merritt, D., & Milosavljević M. 2005, *LRR*, 8, 8
- Miyaji, T., Hasinger, G., & Schmidt, M. 2000, *A&A*, 353, 25
- Myers, A. D., Brunner, R. J., Nichol, R. C., Richards, G. T., Schneider, D. P., & Bahcall, N. A. 2007, *ApJ*, 658, 85
- Miralda-Escudé, J. 2003, *ApJ*, 597, 66
- Monaco, P., & Fontanot, F. 2005, *MNRAS*, 359, 283
- Murray, N., Quataert, E., Thompson, T. A. 2005, *ApJ*, 618, 569
- Nakamura, O., Fukugita, M., Yasuda, N., Loveday, J., Brinkmann, J., Schneider, D. P., Shimasaku, K., & SubbaRao, M. 2003, *AJ*, 125, 1682
- Nandra, K., Mushotzky, R. F., Arnaud, K., Steidel, C. C., Adelberger, K. L., Gardner, J. P., Teplitz, H. I., & Windhorst, R. A. 2002, *ApJ*, 576, 625
- Nandra, K., Laird, E. S., & Steidel, C. C. 2005, *MNRAS*, 360, L39
- Narayan, R., Mahadevan, R., & Quataert, E. 1998, in "The Theory of Black Hole Accretion Discs", eds. M. A. Abramowicz, G. Björnsson, and J. E. Pringle (Cambridge: Cambridge Univ. Press), p.148, *astroph/9803141*
- Netzer, H., Trakhtenbrot, B. 2007, *ApJ*, 654, 754
- Netzer, H., Lira, P., Trakhtenbrot, B., Shemmer, O., & Cury, I. 2007, *ApJ*, 671, 1256
- Osmer, P. S. 2004, in *Carnegie Observatories Astrophysics Series, Vol. 1: Coevolution of Black Holes and Galaxies*, ed. L. C. Ho (Cambridge Univ. Press), in press, *astroph/0304150*
- Pannella, M., Hopp, U., Saglia, R. P., Bender, R., Drory, N., Salvato, M., Gabasch, A., & Feulner, G. 2006, *ApJ*, 639, 1
- Peeples, M. S., & Martini, P. 2006, *ApJ*, 652, 1097
- Pei, Y. C. 1995, *ApJ*, 438, 623
- Peng, C. Y., Impey, C. D., Rix, H. W., Kochanek, C. S., Keeton, C. R., Falco, E. E., Lehar, J., & McLeod, B. A. 2006, *ApJ*, 649, 616
- Polletta, M., Weedman, D., Hoenig, S., Lonsdale, C. J., Smith, H. E., & Houck, J. 2008, *ApJ*, 675, 960
- Porciani, C., Magliocchetti, M., & Norberg, P. 2004 *MNRAS*, 355, 1010
- Porciani, C., & Norberg, P. 2006, *MNRAS*, 371, 1824
- Rees, M. J. 1984, *ARA&A*, 22, 471
- Richards, G. T., et al. 2006, *AJ*, 131, 2766
- Richstone, D., et al. 1998, *Nat*, 395, A14
- Rigby, J. R., Rieke, G. H., Donley, J. L., Alonso-Herrero, A., & Pérez-González, P. G. 2006, *ApJ*, 645, 115
- Salucci, P., Szuszkiewicz, E., Monaco, P., & Danese, L. 1999, *MNRAS*, 307, 637
- Salpeter, E. E. 1964, *ApJ*, 140, 796
- Sanders, D. B., et al. 1988, *ApJ*, 325, 74
- Schirber, M., & Bullock, J. S. 2003, *ApJ*, 584, 110
- Shankar, F., Salucci, P., Granato, G. L., De Zotti, G., & Danese, L. 2004, *MNRAS*, 354, 1020 (S04)
- Shankar, F., Lapi, A., Salucci, P., De Zotti, G., & Danese, L. 2006, *ApJ*, 643, 14
- Shankar, F., & Mathur, S. 2007, *ApJ*, 660, 1051
- Shankar, F., & Ferrarese, L. 2008, *ApJ*, submitted
- Shankar, F., Bernardi, M., & Zoltan, H. 2008, *ApJ*, submitted
- Shapiro, S. L. 2005, *ApJ*, 620, 59
- Shen, Y., et al. 2007a, *AJ*, 133, 2222
- Shen, Y., Greene, J. E., Strauss, M., Richards, G. T., & Schneider, D. P. 2007b, *ApJ*, submitted, *arXiv/0709.3098*
- Sheth, R. K., & Tormen, G. 1999, *MNRAS*, 308, 119
- Sheth, R. K., Hui, L., Diaferio, A., & Scoccimarro, R. 2001, *MNRAS*, 325, 1288
- Sheth, R. K., et al. 2003, *ApJ*, 594, 225
- Shields, G. A., Menezes, K. L., Massart, C. A., & Vanden Bout, P. 2006, *ApJ*, 641, 683
- Shinozaki, K., Miyaji, T., Ishisaki, Y., Ueda, Y., & Ogasaka, Y. 2006, 131, 2843
- Silverman, J. D., et al. 2008, *ApJ*, 679, 118
- Small, T. A., & Blandford, R. D. 1992, *MNRAS*, 259, 725
- Smith, R. E., Peacock, J. A., Jenkins, A., White, S. D. M., Frenk, C. S., Pearce, F. R., Thomas, P. A., Efstathiou, G., & Couchman, H. M. P. 2003, *MNRAS*, 341, 1311
- Soltan, A. 1982, *MNRAS*, 200, 115
- Steed, A., & Weinberg, D. H. 2003, *astroph/0311312* (SW03)
- Steffen, A. T., Strateva, I., Brandt, W. N., Alexander, D. M., Koekemoer, A. M., Lehmer, B. D., Schneider, D. P., & Vignali, C. 2006, *AJ*, 131, 2826
- Steidel, C. C., Hunt, M. P., Shapley, A. E., Adelberger, K. L., Pettini, M., Dickinson, M., & Giavalisco, M. 2002, *ApJ*, 576, 653
- Stern, D., et al. 2005, *ApJ*, 631, 163
- Tacconi, L. J., Neri, R., Chapman, S. C., Genzel, R., Smail, I., Ivison, R. J., Bertoldi, F., Blain, A., Cox, P., Greve, T., Omont, A. 2006, 640, 228
- Tamura, N., Ohta, K., & Ueda, Y. 2006, *MNRAS*, 365, 134
- Tinker, J. L., Weinger, D. H., Zheng, Z., & Zehavi, I. 2005, *ApJ*, 631, 41
- Tonry, J., et al. 2001, *ApJ*, 546, 681
- Tozzi, P., et al. 2006, *A&A*, 451, 457
- Treister, E., et al. 2006, *ApJ*, 640, 603
- Treu, T., Ellis, R. S., Liao, T. X., van Dokkum, P. G., Tozzi, P., Coil, A., Newman, J., Cooper, M. C., & Davis, Marc 2005, *ApJ*, 633, 174
- Tundo, E., Bernardi, M., Hyde, J. B., Sheth, R. K., & Pizzella, A. 2007, *ApJ*, 663, 53
- Ueda, Y., Akiyama, M., Ohta, K., & Miyaji, T. 2003, *ApJ*, 598, 886 (U03)
- Vale, A., & Ostriker, J. P. 2004, *MNRAS*, 353, 189
- Vestergaard, M. 2004, *ApJ*, 601, 676
- Vittorini, V., Shankar, F., & Cavaliere, A. 2005, *MNRAS*, 363, 1376
- Volonteri, M., Madau, P., & Haardt, F. 2003, *ApJ*, 593, 661
- Volonteri, M., Madau, P., Quataert, E., & Rees, M. J. 2005, *ApJ*, 620, 69
- Volonteri, M., Salvaterra, R., & Haardt, F. 2006, *MNRAS*, 373, 121
- Wilman, R. J., & Fabian, A. C. 1999, *MNRAS*, 309, 862
- Wisotzki, L. 1999, *Reviews in Modern Astronomy* 12, *Astronomical Instruments and Methods at the turn of the 21st Century*. Edited by Reinhard E. Schielicke. Published by Astronomische Gesellschaft, Hamburg, p. 231
- Wolf, C., et al. 2003, *A&A*, 408, 499
- Wyithe, J. S. B. 2004, *MNRAS*, 1082, 1098
- Yoo, J., & Miralda-Escudé, J. 2004, *ApJ*, 614, 25
- Yoo, J., Miralda-Escudé, J., Weinberg, D. H., Zheng, Z., & Morgan, C. W. 2007, *ApJ*, submitted, *astroph/0702199*
- Yu, Q., & Lu, Y. 2004, *ApJ*, 602, 603
- Yu, Q., & Tremaine, S. 2002, *MNRAS*, 335, 965

TABLE 1
AGN LUMINOSITY FUNCTION PARAMETERS

Parameter						
p_1	4.23 ($z < 4$)	$-0.615z + 6.690$	3.0 ($z = 6$)			
p_2	-1.5 at all z					
γ_1	0.86 at all z					
γ_2	2.6 ($z < 0.5$)	$-0.933z + 3.067$	2.32 ($0.8 < z < 4$)	$0.24z + 1.36$	2.8 ($z = 6$)	
A	$5.04 \times 10^{-6} \text{ Mpc}^{-3}$					
z_c^*	1.9					
$\log L_a$	44.6 ($z < 3$)	$0.0667z + 44.4$	44.8 ($z = 6$)			
$\log L_*$	43.94					

NOTE. — List of the parameters entering the AGN luminosity function described in § 2. Some of the parameters assume different values in different redshift bins as quoted. A smooth linear transition in redshift z in the values has been applied between discontinuous redshift bins. Luminosities are the inferred values in the 2–10 keV band, in units of erg s^{-1} .

TABLE 2
AGN BOLOMETRIC LUMINOSITY FUNCTIONS

z (1)	$\log L$ (2)	$\log \Phi$ (3)	$\log \Phi_{\text{noCT}}$ (4)	$\log \Phi_{\text{DoubleCT}}$ (5)	$\log \Phi_{\text{HRH07}}$ (6)
0.020	41.00	-1.859	-1.994	-1.757	-1.374
0.020	41.25	-2.074	-2.208	-1.972	-1.578
.....					
0.020	48.00	-10.08	-10.16	-10.01	-9.539
0.260	41.00	-1.903	-2.036	-1.796	-1.609
0.260	41.25	-2.089	-2.222	-1.984	-1.787
0.260	41.50	-2.267	-2.399	-2.162	-1.967
.....					

NOTE. — (1) redshift; (2) bolometric luminosity in logarithmic scale in units of erg s^{-1} ; (3) reference bolometric AGN luminosity function in logarithmic scale in units of $\text{Mpc}^{-3} \text{ dex}^{-1}$; (4) reference bolometric AGN luminosity function with no Compton-thick sources (i. e., with $\log N_H/\text{cm}^{-2} > 24$); (5) reference bolometric AGN luminosity function with Double contribution from Compton-thick sources (i. e., with $\log N_H/\text{cm}^{-2} \leq 26$); (6) bolometric AGN luminosity function from HRH07. The full table is available in electronic form.

TABLE 3
BLACK HOLE MASS FUNCTIONS

z (1)	$\log M_\bullet$ (2)	$\log \Phi$ (3)	$\log \Phi_{\text{noCT}}$ (4)	$\log \Phi_{\text{DoubleCT}}$ (5)	$\log \Phi_{\text{HRH07}}$ (6)	$\log \Phi_{\text{HRH07EXTRA}}$ (7)
0.02	5.0	-1.264	-1.398	-1.162	-0.928	-0.952
0.02	5.2	-1.394	-1.528	-1.292	-1.060	-1.082
.....						
0.02	9.6	-4.683	-4.779	-4.604	-4.436	-4.964
0.26	5.0	-1.482	-1.614	-1.376	-1.129	-1.131
0.26	5.2	-1.608	-1.739	-1.501	-1.247	-1.248
0.26	5.4	-1.723	-1.855	-1.616	-1.365	-1.364
.....						

NOTE. — (1) redshift; (2) black hole mass in logarithmic scale in units of M_\odot ; (3) black hole mass function in our reference model in logarithmic scale in units of $\text{Mpc}^{-3} \text{ dex}^{-1}$; (4) reference black hole mass function in the same model but with no Compton-thick sources; (5) reference black hole mass function in the same model but with Double contribution from Compton-thick sources; (6) black hole mass function in the same model but adopting the HRH07 luminosity function; (7) black hole mass function obtained adopting the HRH07 luminosity function with $\epsilon = 0.09$ and $\dot{m} = 1$, as in Figure 8d. The full table is available in electronic form.

TABLE 4
BLACK HOLE DUTY CYCLES

z (1)	$\log M_{\bullet}$ (2)	P_0 (3)	P_0^{noCT} (4)	P_0^{DoubleCT} (5)	P_0^{HRH07} (6)	$P_0^{\text{HRH07EXTRA}}$ (7)
0.02	5.0	0.00995	0.00995	0.00995	0.01401	0.00727
0.02	5.2	0.00941	0.00942	0.00942	0.01299	0.00668
.....						
0.02	9.6	0.00008	0.00008	0.00008	0.00011	0.00009
0.26	5.0	0.03063	0.03057	0.03050	0.01947	0.01050
0.26	5.2	0.03246	0.03231	0.03215	0.01837	0.00987
0.26	5.4	0.03273	0.03243	0.03212	0.01729	0.00924
.....						

NOTE. — (1) redshift; (2) black hole mass in logarithmic scale in units of M_{\odot} ; (3) duty cycle for our reference model; (4) duty cycle for the reference model with no Compton-thick sources; (5) duty cycle for the reference model with Double contribution from Compton-thick sources; (6) duty cycle for the model obtained adopting the HRH07 luminosity function; (7) duty cycle for the model obtained adopting the HRH07 luminosity function with $\epsilon = 0.09$ and $\dot{m} = 1$. The full table is available in electronic form.

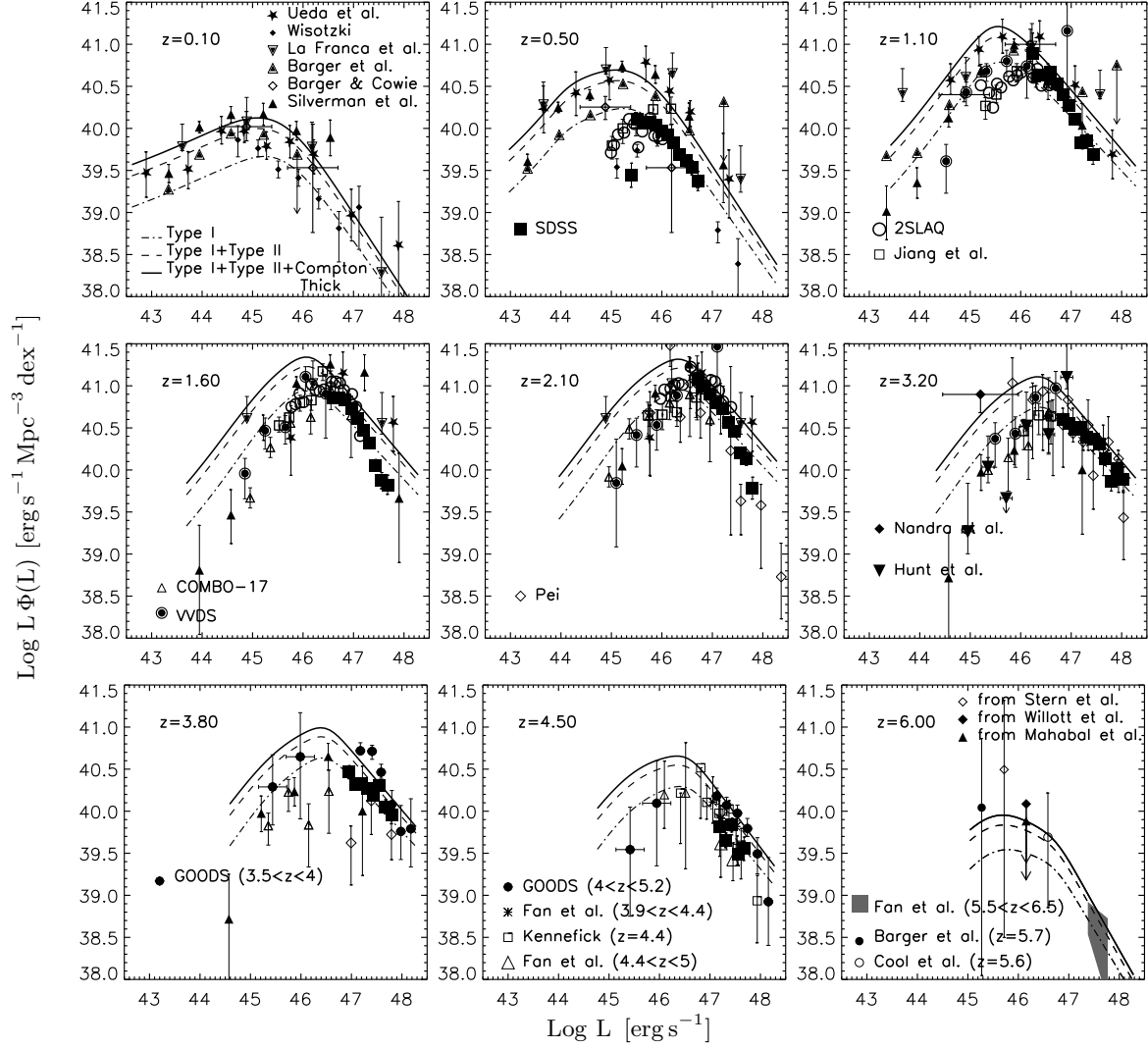


FIG. 1.— The bolometric AGN luminosity function. Curves show the model described in § 2. The *solid* line is the total LF including very Compton-thick sources, the *short-dashed* line includes sources with column densities up to $\log N_H/\text{cm}^{-2} = 24$, while the *dot-dashed* line includes only sources with $\log N_H/\text{cm}^{-2} \leq 22$. The data from optical surveys are from Hunt et al. (2004), Pei (1995), Wisotzki (1999), Jiang et al. (2006), Cool et al. (2006), Shankar & Mathur (2007; derived from data of Stern et al. 2000; Willott et al. 2004; Mahabal et al. 2005), VIMOS-VLT Deep Survey (Bongiorno et al. 2007), 2SLAQ (Richards et al. 2005), SDSS (Richards et al. 2006; Fan et al. 2001, 2004), COMBO-17 (Wolf et al. 2003), Kennefick et al. (1994). The data from X-ray surveys are from Ueda et al. (2003), Barger et al. (2003), Barger et al. (2005), Barger & Cowie (2005), Nandra et al. (2005) and Silverman et al. (2008). GOODS (multi-wavelength) data are from Fontanot et al. (2007).

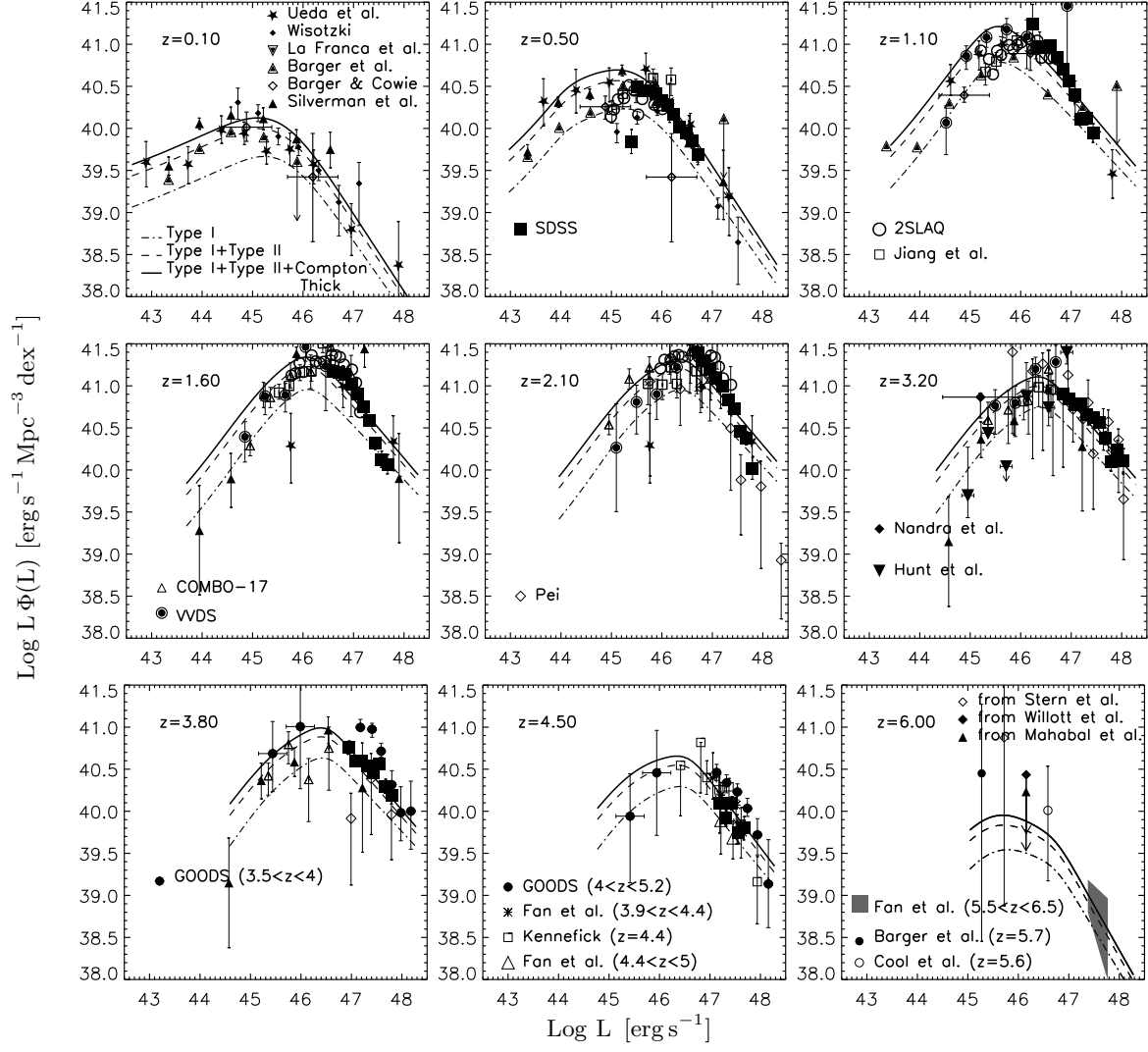


FIG. 2.— Same as Figure 1 but now all the data have been corrected for the obscured fraction as given in HRH07.

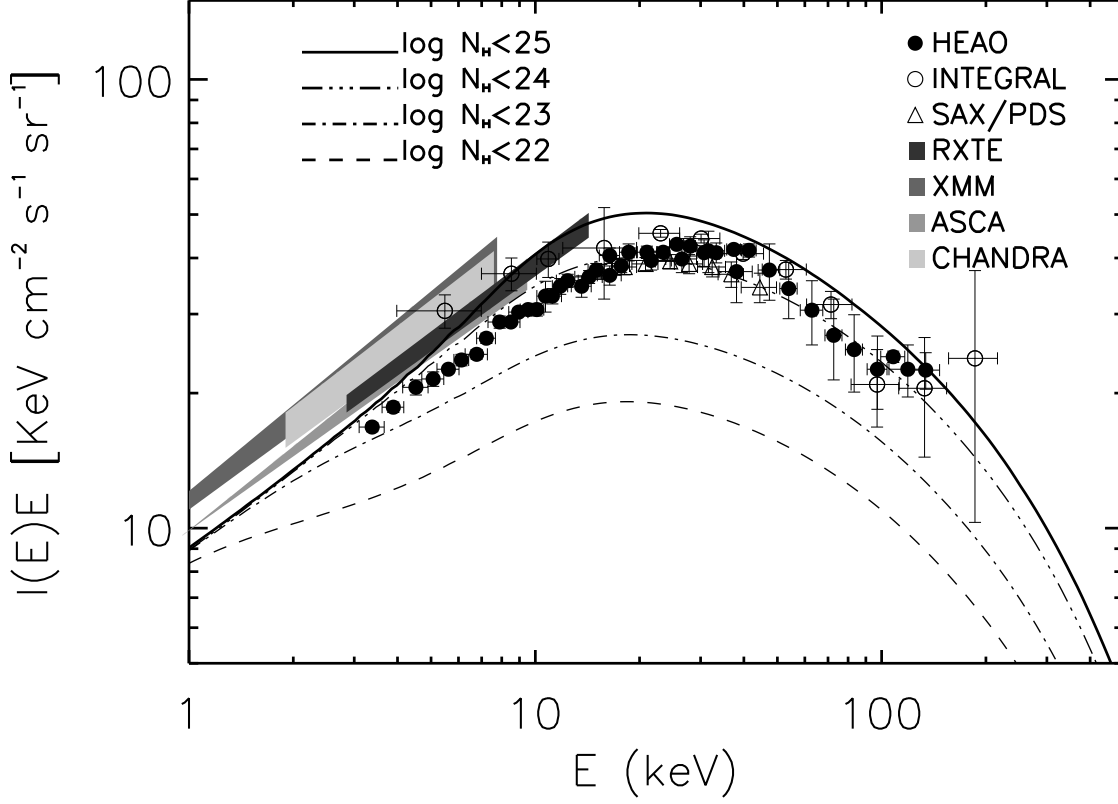


FIG. 3.— The X-ray background. Curves represent the integration of our AGN bolometric LF converted to hard X-ray bands, as described in the text. The *dashed* line includes sources with column densities up to $\log N_H/\text{cm}^{-2} \leq 22$, the *dot-dashed* line those up to $\log N_H/\text{cm}^{-2} \leq 23$, and the *triple-dot dashed* line those with $\log N_H/\text{cm}^{-2} \leq 24$. The *solid* line refers to the total when including Compton-thick sources up to $\log N_H/\text{cm}^{-2} \leq 25$, with a dependence on luminosity following that in U03. Data are taken from a compilation in Frontera et al. (2007).

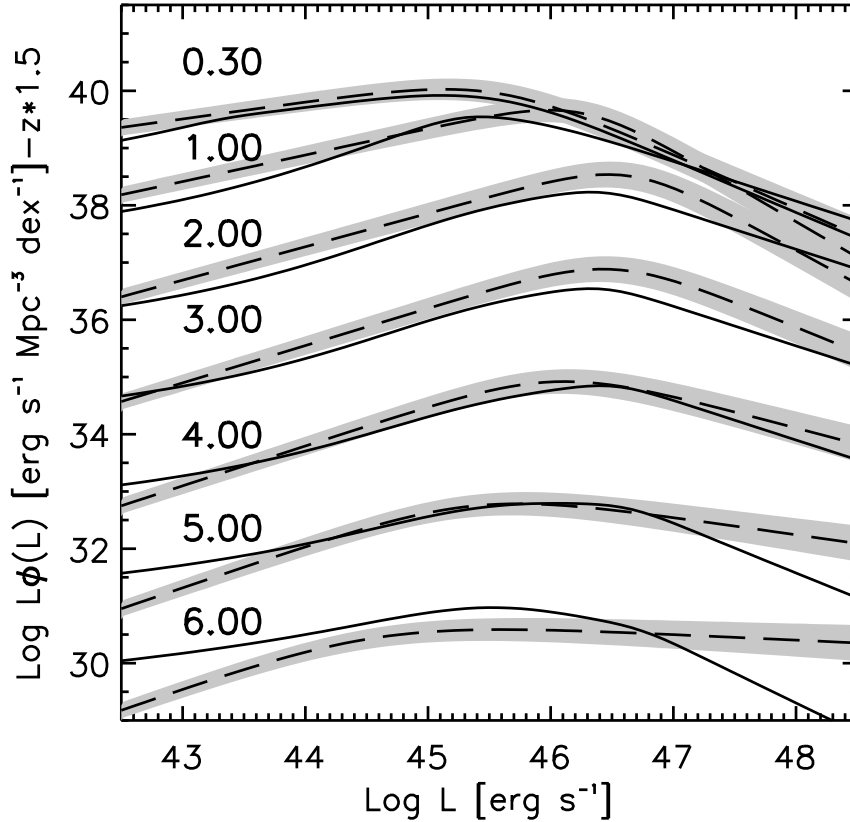


FIG. 4.— Comparison between the bolometric AGN luminosity function described in § 2 (*solid* line) and the recently derived estimate by HRH07 (*dashed* line), shown with its 1- σ uncertainty in the bolometric correction (*gray area*). Curves are vertically offset by $-1.5 \times z$.

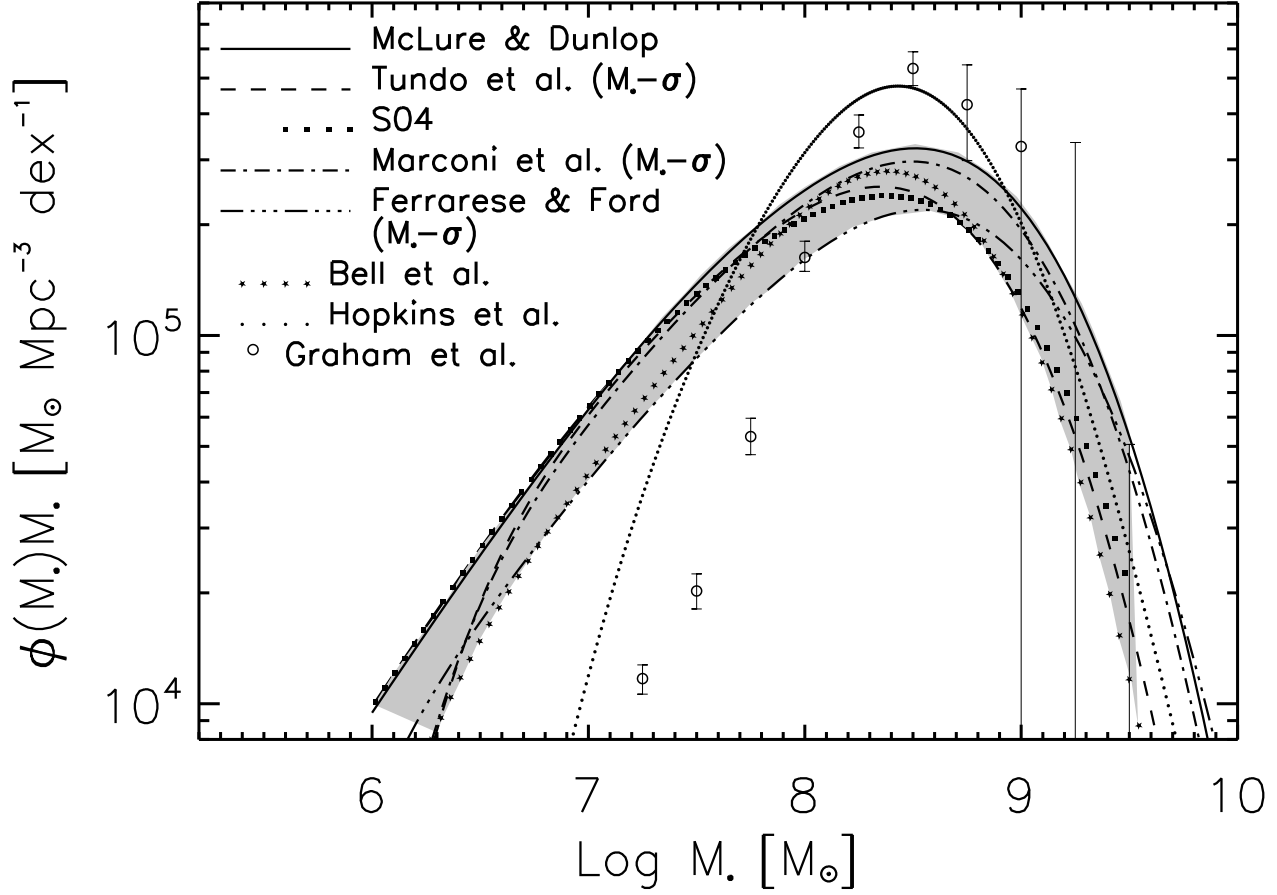


FIG. 5.— Comparison among estimates of the local black hole mass function. Lines show estimates using various calibrations of the $M_{\bullet} - L_{\text{sph}}$, $M_{\bullet} - \sigma$, or $M_{\bullet} - M_{\text{star}}$ relations as described in the text, assuming a 0.3-dex intrinsic scatter in all cases. The grey band encompasses the range of these estimates. Filled small circles show the determination of Hopkins et al. (2007b) using the black hole “fundamental plane” and open circles show the determination of Graham et al. (2007) using the relation between black hole mass and Sérsic index.

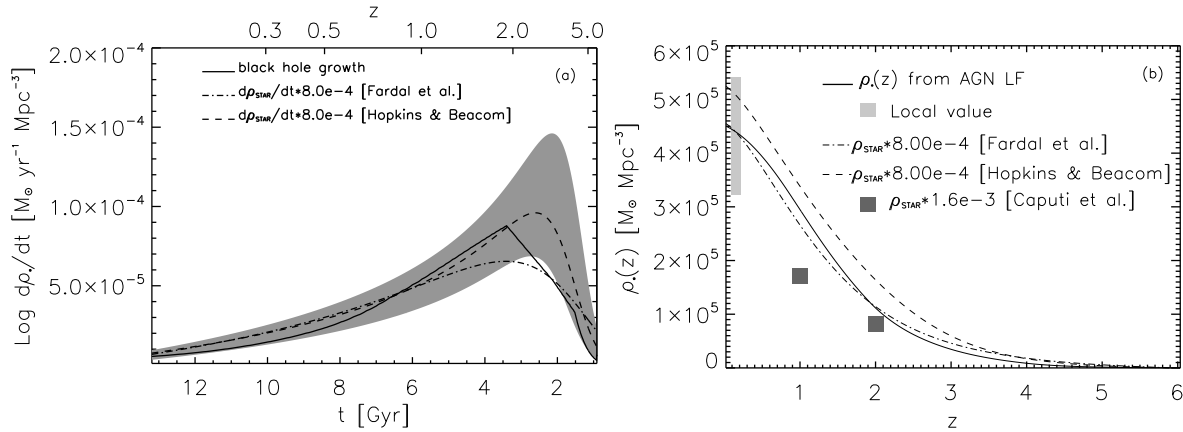


FIG. 6.— Black hole growth and stellar mass growth. (a) Average black hole accretion rate as computed via equation (4) compared to the SFR as given by Hopkins & Beacom (2006) and Fardal et al. (2007), scaled by the factor $M_{\bullet}/M_{\text{STAR}} = 0.5 \times 1.6 \times 10^{-3}$. The grey area shows the 3- σ uncertainty region from Hopkins & Beacom (2006). (b) Cumulative black hole mass density as a function of redshift. The solid line is the prediction based on the bolometric AGN luminosity function. The *light-gray area* is the local value of the black hole mass density with its systematic uncertainty as given in Figure 5. The *dark squares* are estimates of the black hole mass function at $z = 1$ and $z = 2$ obtained from the stellar mass function of Caputi et al. (2006) and Fontana et al. (2006), scaled by the local ratio $M_{\bullet}/M_{\text{STAR}} = 1.6 \times 10^{-3}$. The lines are the integrated stellar mass densities based on the SFR histories in panel (a), scaled by 8×10^{-4} .

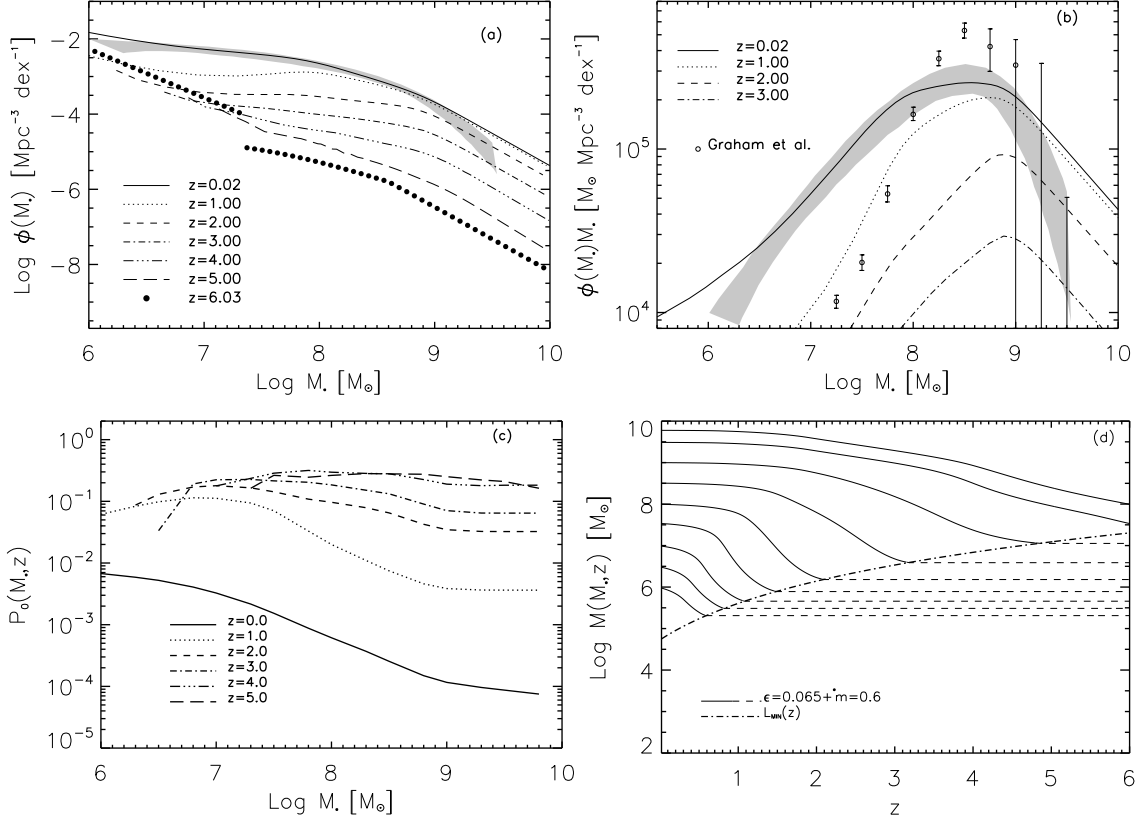


FIG. 7.— Results for a reference model that agrees well with the local black hole mass function, with $\epsilon = 0.065$, $m_0 = 0.60$, and an initial duty cycle $P_0(z = 6) = 0.5$. (a) The accreted mass function shown at different redshifts as labeled, compared with the local mass function (grey area). (b) Similar to (a) but plotting $M_* \Phi(M_*)$ instead of $\Phi(M_*)$. (c) Duty-cycle as a function of black hole mass and redshift as labeled. (d) Average accretion histories for black holes of different relic mass M_* at $z = 0$ as a function of redshift; the dashed lines represent the curves when the black hole has a luminosity below $L_{\text{MIN}}(z)$ and therefore does not grow in mass; the minimum black hole mass corresponding to $L_{\text{MIN}}(z)$ at different redshifts is plotted with a dot-dashed line.

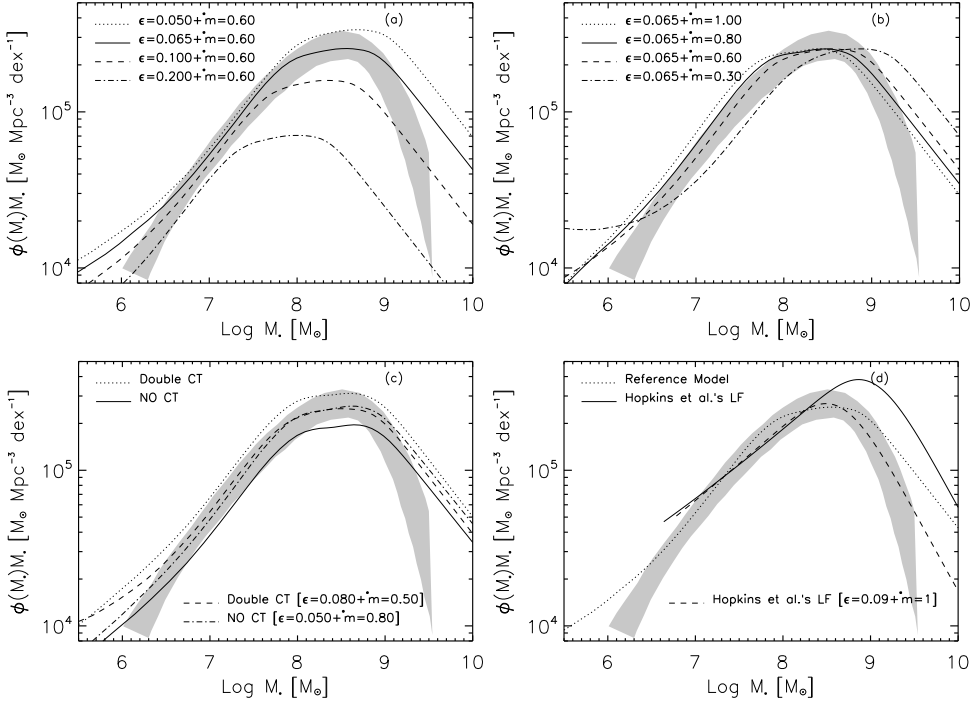


FIG. 8.— Effect of model inputs on the predicted black hole mass function at $z = 0$. (a) Varying ϵ at fixed $m_0 = 0.60$. (b) Varying m_0 at fixed $\epsilon = 0.065$. (c) Solid and dotted curves show the effect of removing or doubling the fraction of Compton-thick sources, keeping $\epsilon = 0.065$ and $m_0 = 0.60$ fixed at their reference values. Dashed and dot-dashed curves show these modified models with parameter values chosen to reproduce the local mass function. (d) The solid curve shows the effect of adopting the HRH07 LF, with $\epsilon = 0.065$ and $m_0 = 0.60$. The dashed curve shows a model with the HRH07 LF and parameter values $\epsilon = 0.09$ and $m_0 = 1$.

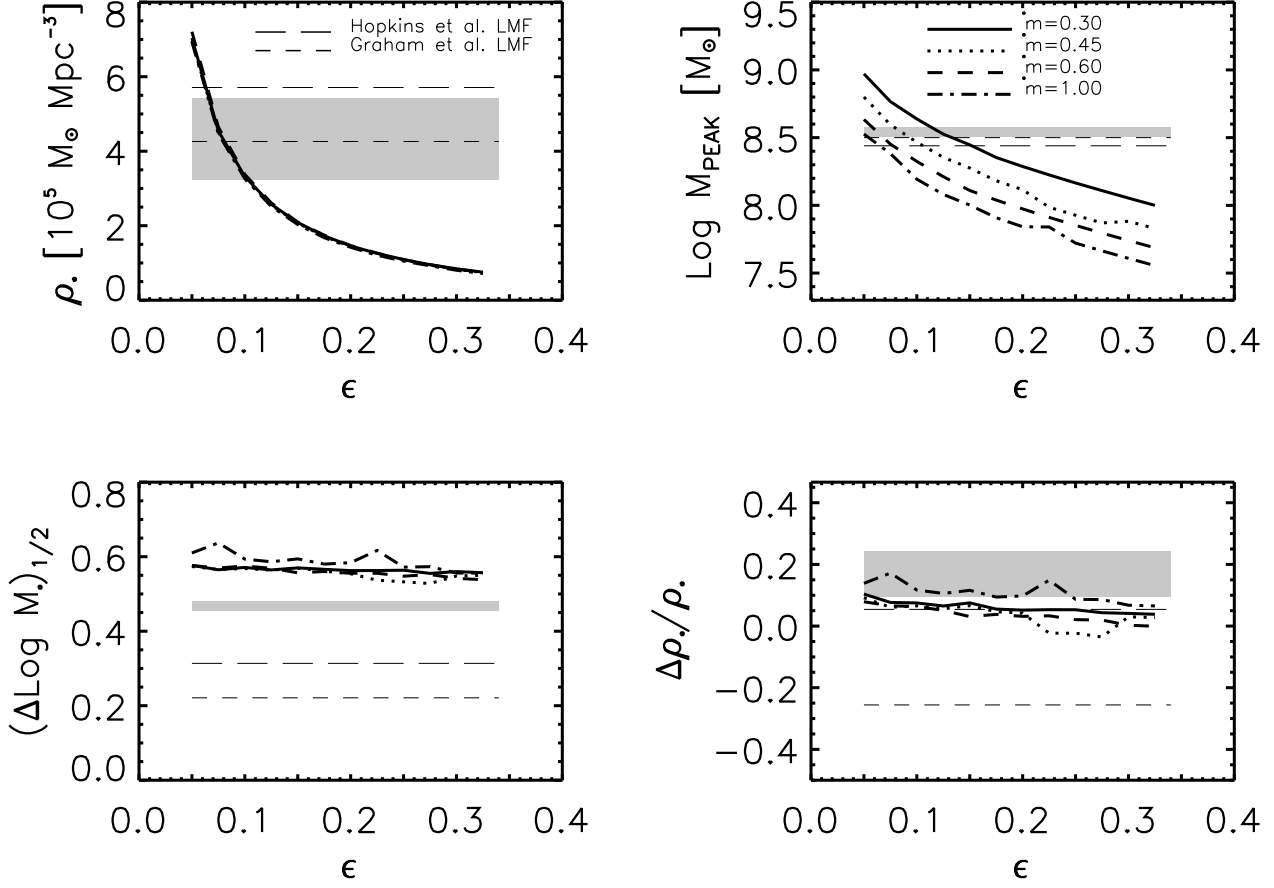


FIG. 9.— Models incorporating our standard luminosity function estimate compared to the properties of the local black hole mass function described in § 4.3: integrated mass density (ρ_{\bullet} , upper left), peak mass (M_{PEAK} , upper right), width ($M_{\bullet,1/2}$, lower left), and asymmetry ($\Delta \rho_{\bullet} / \rho_{\bullet}$, lower right). The *thick* lines show model predictions as a function of radiative efficiency ϵ , for several values of m_0 as labeled. The horizontal *grey band* shows observational estimates of the four quantities based on the grey band in Figure 5. Horizontal *long-dashed* and *short-dashed* lines show the values derived from the local mass functions of Hopkins et al. (2007b) and Graham et al. (2007), respectively.

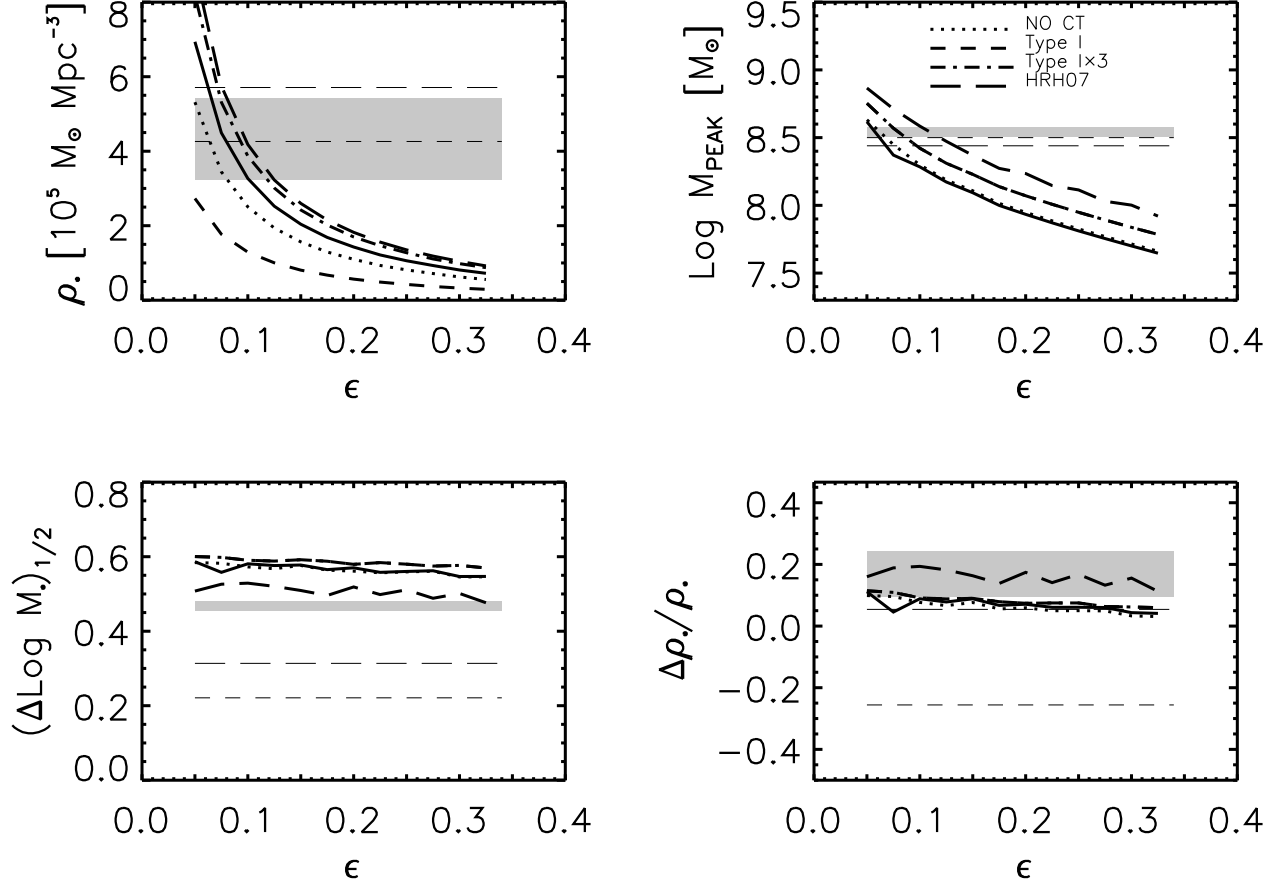


FIG. 10.— Local black hole mass function parameters predicted for different LF inputs. The accretion rate is fixed to $\dot{m}_0 = 0.75$ in all cases. The *thick* lines refer to models with our standard LF estimate (*solid* line), with no contribution of Compton-thick sources (*dotted* line), with only Type I AGNs included (*dashed* line), with Type I AGNs multiplied by a constant factor of 3 at all redshifts and all luminosities (*dot-dashed* line), and with the HRH07 LF (*long-dashed* line). Grey band and horizontal thin lines are as in Figure 9.

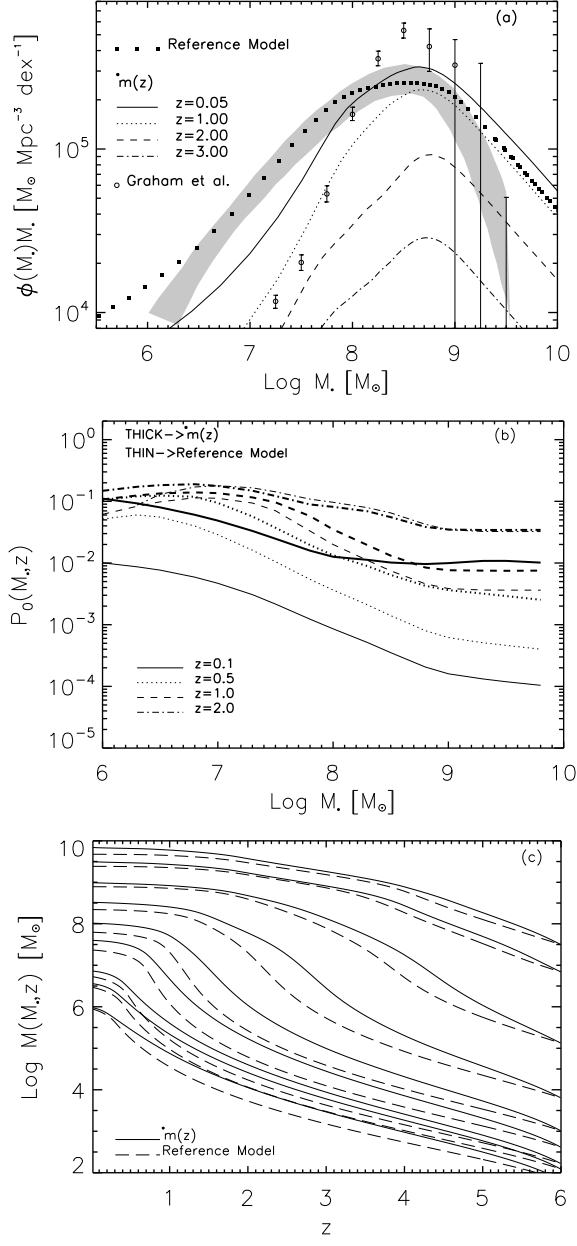


FIG. 11.— Model with $\epsilon = 0.065$ and decreasing $\dot{m}_0(z)$ as given in equation (17), compared to our reference model with constant $\dot{m}_0 = 0.6$ and $\epsilon = 0.065$. Panels (a), (b), (c) show, respectively, the evolution of the mass function, the evolution of the duty cycle, and mass growth along characteristics, in the same format as Figure 7. Reference model results are shown by *squares* in (a), by *thinner lines* in (b), and by *long-dashed lines* in (c).

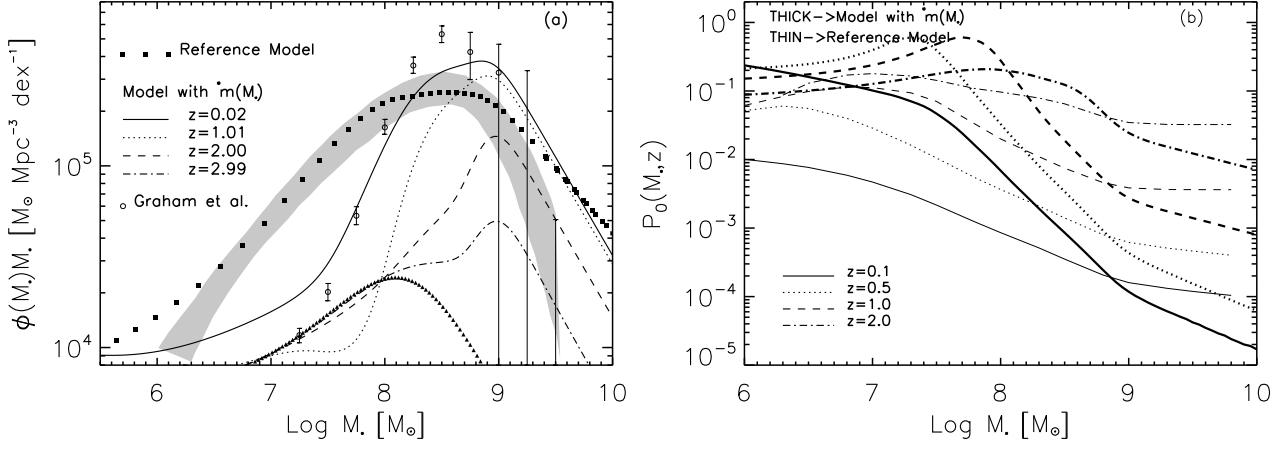


FIG. 12.— Model with $\epsilon = 0.075$ and a mass-dependent Eddington ratio $\dot{m}_0 = 0.445(M_\bullet/10^9 M_\odot)^{0.5}$ (equation 18), compared to our reference model. The format is similar to panels (a) and (b) of Figure 11.

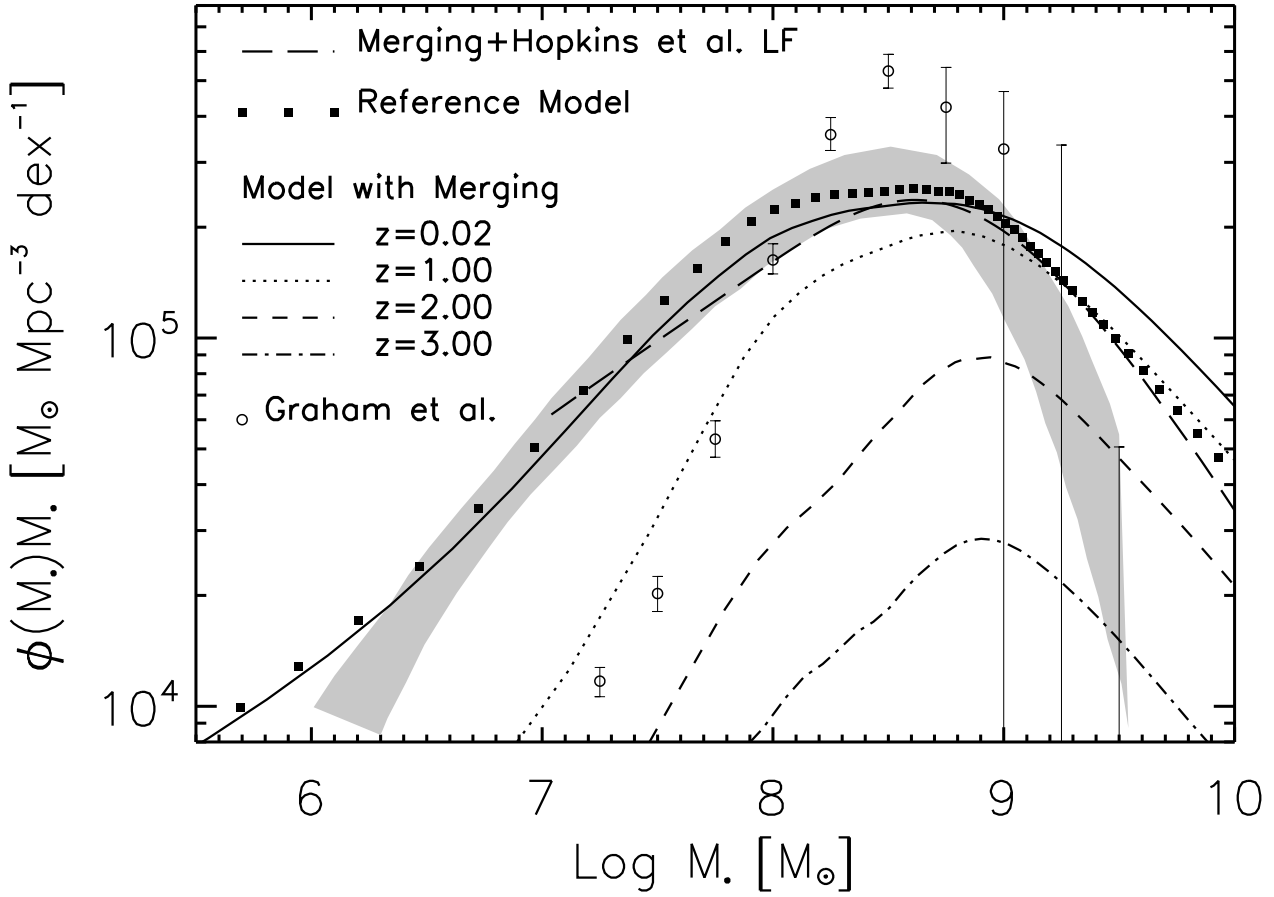


FIG. 13.— Evolution of the black hole mass function in a model with black hole mergers. Accretion-driven growth is computed assuming $\epsilon = 0.065$, $\dot{m}_0 = 0.60$, and each black hole has a probability $P_{\text{merg}} = 0.5$ of merging with another black hole of equal mass per Hubble time $t_H(z)$. Squares show the $z = 0$ predictions of the reference model (same accretion parameters, no merging), and the long-dashed line shows the $z = 0$ mass function for a merger model with the HRH07 LF and accretion parameters $\epsilon = 0.09$, $\dot{m}_0 = 1$.

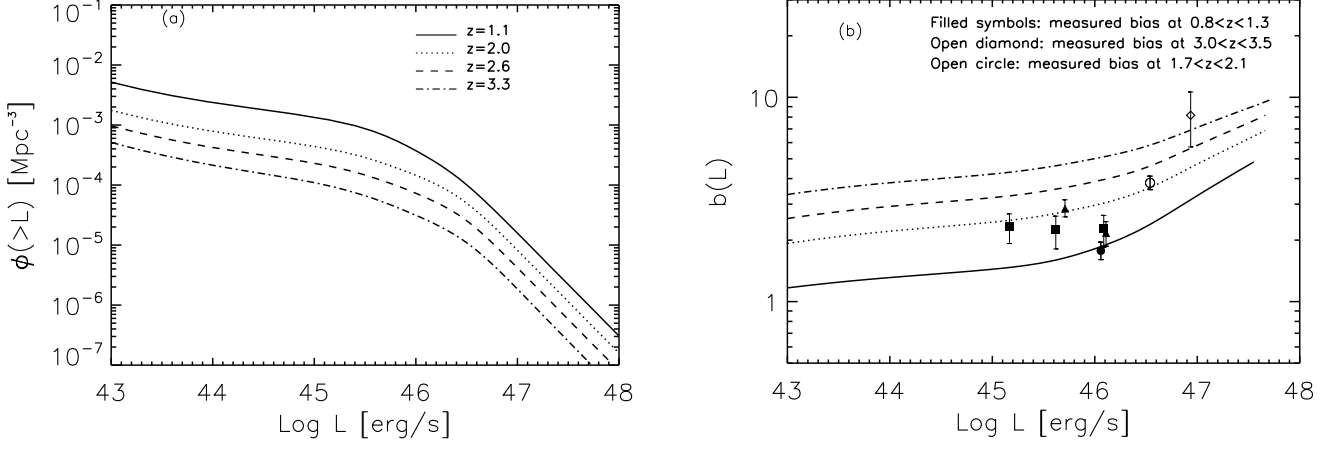


FIG. 14.— Panel *a*: cumulative space density of predicted hosts (including those with inactive black holes of the same mass) that have a luminosity higher than L for four different redshifts. Panel *b*: predicted bias as a function of luminosity and redshift, computed according to equations (22) and (23); the data are from da Angela et al. (2006; *filled triangles*), Myers et al. (2007; *filled squares*), Porciani & Norberg (2007; *filled and open circles*), and Shen et al. (2007a; *open diamonds*), all corrected to $\sigma_8 = 0.8$. Both panels refer to the predictions of our reference model.